JGR Oceans

RESEARCH ARTICLE
10.1029/2020JC016501

Key Points:

- Regional nitrogen availability in the Arctic Ocean is an important factor determining the physiological status of phytoplankton
- Severe nitrogen limitation reduces gross photosynthetic rates of phytoplankton in the western Arctic Ocean in summer by approximately 40%
- Large-sized phytoplankton are more susceptible to nitrogen stress in the Arctic Ocean

Supporting Information:

- Supporting Information S1

Correspondence to:
J. Park,
jspark@kopri.re.kr

Citation:
Ko, E., Gorbunov, M. Y., Jung, J., Joo, H. M., Lee, Y., Cho, K.-H., et al. (2020). Effects of nitrogen limitation on phytoplankton physiology in the western Arctic Ocean in summer. *Journal of Geophysical Research: Oceans*, *125*, e2020JC016501. https://doi.org/10.1029/2020JC016501

Received 14 JUN 2020
Accepted 20 OCT 2020
Accepted article online 22 OCT 2020

Effects of Nitrogen Limitation on Phytoplankton Physiology in the Western Arctic Ocean in Summer

Eunho Ko[1,2], Maxim Y. Gorbunov[3], Jinyoung Jung[1], Hyoung Min Joo[1], Youngju Lee[1], Kyoung-Ho Cho[1], Eun Jin Yang[1], Sung-Ho Kang[1], and Jisoo Park[1,2]

[1]Division of Polar Ocean Sciences, Korea Polar Research Institute, Incheon, Republic of Korea, [2]University of Science and Technology, Daejeon, Republic of Korea, [3]Department of Marine and Coastal Science, Rutgers University, New Brunswick, NJ, USA

Abstract Phytoplankton in the Arctic Ocean are subject to nitrogen limitation in the summer, however, how severely the nitrogen stress affects phytoplankton physiology remains largely unknown. In the summers of 2015–2018, we examined the distribution of phytoplankton photophysiological properties across two contrasting regions of the Arctic Ocean with distinctly different levels of nitrogen availability in the upper water column. We quantified the extent of nitrogen stress using a highly sensitive fluorescence induction and relaxation system to obtain continuous underway measurements and via discrete sample analyses of phytoplankton physiology, as well as nutrient enrichment incubations. The results revealed vast regions in the Chukchi Sea where phytoplankton photosynthesis was severely nitrogen-stressed. Thereby, the maximum quantum yield of photochemistry in photosystem II showed only a small decrease (12 ± 9%) relative to its nutrient-replete values, while the maximum photosynthetic electron transport rates under saturating irradiance were impaired to a greater extent (40 ± 17%). This phytoplankton photosynthesis response is indicative of a severe nitrogen limitation, which results in dramatic reduction in growth and net primary production rates. Nutrient enrichment incubations also revealed a marked increase in large-size phytoplankton growth (>10 μm) after the nitrogen stress was alleviated, suggesting that the larger cells were more susceptible to nitrogen stress. These results are important for understanding how regional nitrogen fluxes control variability in the primary production and phytoplankton community structure and how these processes might change with rapid climate changes in the Arctic Ocean.

Plain Language Summary Nutrient availability is the main bottom-up controls of phytoplankton physiology and growth in the upper ocean. The distribution of nutrient limitation in the global ocean varies greatly in space and time, so phytoplankton responses to this factor are essential for understanding the marine ecosystem. Although nitrogen limitation was previously shown in the Arctic Ocean in the summer, how nitrogen stress affects phytoplankton physiology remains largely unknown. This study investigates, with high spatial resolution, the distribution of phytoplankton physiological status and quantifies the effects of nitrogen stress in the western Arctic Ocean. Our results revealed severe nitrogen limitation in the summer that results in dramatic reduction in growth and net primary production in this region of the ocean. Therefore, alterations in nitrogen fluxes along with climate change in the Arctic Ocean would be important for controlling phytoplankton growth and primary production in this region.

1. Introduction

The Arctic Ocean is exposed to dramatic climate changes, which have resulted in increasing river runoff and water temperatures, melting sea ice, and reduced amounts of permafrost (Graversen et al., 2008; Serreze & Stroeve, 2015; Wassmann et al., 2011). Recent changes in the marine environment have a profound impact on the Arctic Ocean's biogeochemical cycle. For example, increasing water temperature directly influences biological activity and metabolism rates (Coello-Camba & Agustí, 2017; Sugie et al., 2020). The increased amount of fresh water generated by melting sea ice and increased river runoff has enhanced the stratification in the ocean's upper layer (Frey et al., 2014; Screen & Simmonds, 2010; Timmermans et al., 2011), hindering the supply of nutrients from the deeper layers to the surface (Carmack et al., 2016). In addition, as the trend shifted from multiyear ice to 1-year ice in the Arctic Ocean, the increase in light transmission to the upper layer has an impact on reducing light absorption capacity of phytoplankton and increasing photoprotective xanthophyll pigments due to photoinhibition in spring (Lewis et al., 2019). Meanwhile, increased turbulence, caused by upwelling in the coastal waters due to climate changes, is likely to supply nutrients and trace metal through transport polar drift to the Arctic Ocean shelf and central basin (Kipp et al., 2018). Remote sensing data have shown a tendency of earlier phytoplankton blooms and increased primary production owing to continued decrease in sea ice in the Arctic Ocean over the past few decades (Arrigo et al., 2008; Arrigo & van Dijken, 2015). However, the physiological response of phytoplankton to specific environmental factors can only be inferred from in situ data. To forecast how phytoplankton productivity could change in the future, it is important to elucidate how environmental factors affect the growth and physiological state of phytoplankton in the Arctic Ocean.

Phytoplankton rapidly adapt their physiological status to the surrounding environment; hence, the physiological responses of organisms vary greatly in time and space (Cloern et al., 1995; Cullen, 1982; Geider, 1987). These changes in phytoplankton physiological characteristics are directly linked to growth and primary productivity (Falkowski et al., 1992; Smith, 1982). The major environmental factors affecting phytoplankton growth are major nutrients, such as nitrate and phosphate (Kulk et al., 2018; Lewis et al., 2019; Mills et al., 2018), light (Zhu et al., 2019), and sometimes the micronutrient iron (Boyd, 2019; Martin et al., 1994; Rijkenberg et al., 2018). As such, one or more limiting factors are simultaneously associated with photosynthetic energy conversion for phytoplankton growth (Arrigo, 2005; Rhee & Gotham, 1981; Xu et al., 2014). However, it is challenging to predict the phytoplankton physiological response to multiple environmental factors, especially when these factors vary in time and space (Moore et al., 2013). Therefore, measurements of an extensive suite of physiological characteristics are needed to quantify the impact of varied environmental conditions on phytoplankton photosynthesis.

The photosynthetic characteristics of phytoplankton can be quantified in real time using variable fluorescence techniques, which have the advantage of being fast and sensitive (Falkowski & Kolber, 1995; Falkowski & Raven, 2007; Suggett et al., 2009). Among these parameters, the maximum quantum yield of photochemistry (F_v/F_m) in photosystem II (PSII) has commonly been used to diagnose nutrient limitations (Falkowski & Raven, 2007; Geider et al., 1993; Kolber et al., 1988). In the case of nitrogen limitation, however, the relationship between F_v/F_m and phytoplankton growth rates is highly nonlinear (Kolber et al., 1988; Parkhill et al., 2001), which makes it impossible to quantify the extent of nitrogen stress from F_v/F_m alone. Nitrogen limitation has stronger impact on the Calvin-Benson cycle, RUBISCO activity (Geider et al., 1993), and photosynthetic electron transport rates ($\mathrm{ETR}^{\mathrm{max}}$) achieved under saturating irradiance, as compared to the maximum quantum yield of photochemistry in PSII, F_v/F_m (Gorbunov & Falkowski, 2020). As a result, a decrease in $\mathrm{ETR}^{\mathrm{max}}$ offers a more sensitive and quantitative diagnostics of nitrogen stress (Gorbunov & Falkowski, 2020).

The photophysiological characteristics of natural phytoplankton assemblages have been evaluated in diverse regions of the ocean, including coastal areas, ocean gyre boundaries, upwellings, and high nutrient low chlorophyll regions. The influence of nutrient limitation on these characteristics is complicated. For instance, field studies have shown that in the North Atlantic, nitrogen limitation may reduce the photochemical efficiency and growth rates of phytoplankton (Graziano et al., 1996). However, nitrate and phosphate simultaneously act as limiting factors for phytoplankton growth in the North Atlantic (Moore et al., 2008). Iron limitation also reduces the energy conversion efficiency in photosynthesis in the equatorial region and South Pacific Ocean (Behrenfeld & Kolber, 1999; Kolber et al., 1988, 1994). Moreover, nutrient uptake rates and carbon-specific photosynthesis vary with changes in the phytoplankton community structure (Cermeño et al., 2005; Hein et al., 1995; Uitz et al., 2008). Recently, the physiological status of phytoplankton in the Arctic Ocean was also known to be affected by light availability and phytoplankton community structure under nitrogen limitation (Kulk et al., 2018; Mills et al., 2018; Mosharov et al., 2019; Zhu et al., 2019). However, these studies were result of a year limited to coastal and shelf regions of the Arctic Ocean, and lacked experimental information on the extent to which physiological conditions were reduced by nitrogen limitation. Larger-scale studies of phytoplankton physiological responses are needed to understand better the variations in phytoplankton biomasses and primary production in relation to environmental changes in the Arctic Ocean.

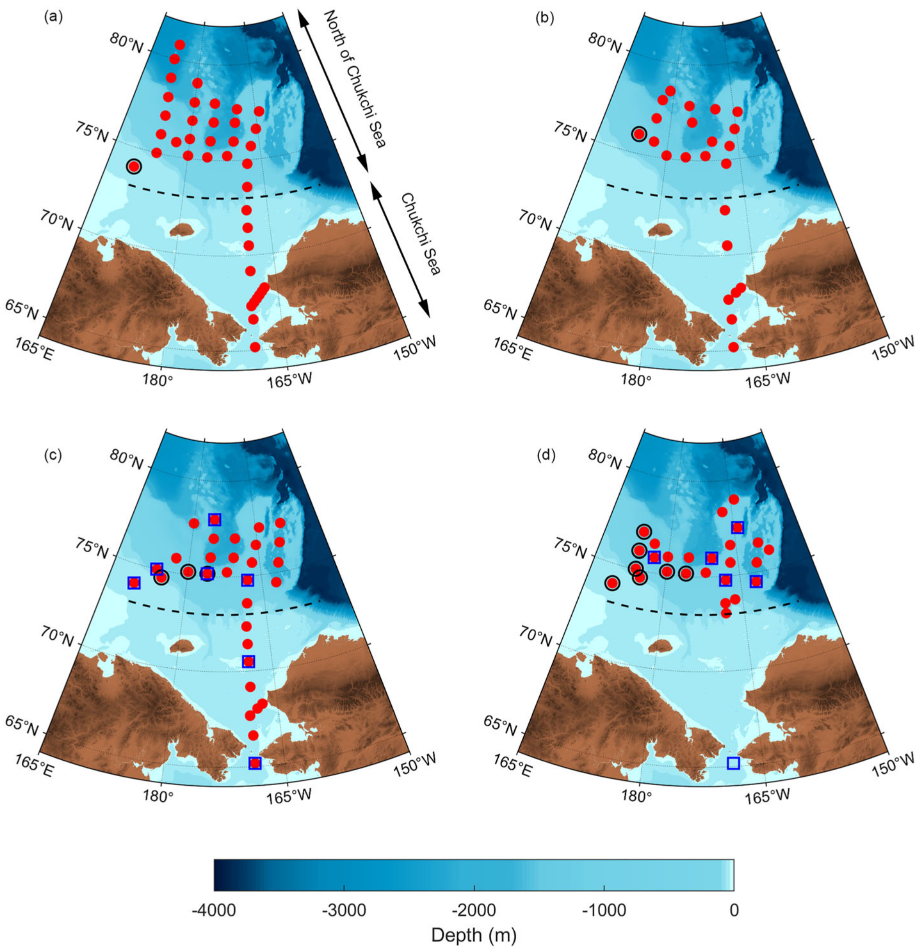

Figure 1. Maps of oceanographic stations in the western Arctic Ocean study area: (a) 2–20 August 2015; (b) 6–19 August 2016; (c) 6–25 August 2017; (d) 6–24 August 2018. Red circles represent stations of each cruise. Blue squares are the stations where incubation experiments were conducted, and black circles indicate the high chlorophyll-a regions in the north of Chukchi Sea. Shading blue represents isobaths. The boundary (73°N) between the Chukchi Shelf and north of the Chukchi Sea is marked by black dashed line.

The goals of this study were to (1) evaluate the phytoplankton photophysiological characteristics during summer in diverse environments of the western Arctic Ocean and (2) quantify their photophysiological responses to nitrate availability. Additionally, this study aimed at elucidating the relationship between photophysiological characteristics and phytoplankton community size structure. To achieve these goals, we investigated the photochemical efficiencies and photosynthesis-versus-irradiance (P-E) parameters in a wide range of waters from the Bering Strait to the northern part of the Chukchi Sea. In addition, shipboard incubations were conducted to quantify the phytoplankton physiological response to nutrient enrichment. This study also identified how the biomass, phytoplankton photophysiological responses, and phytoplankton community size structure were affected by nitrogen limitation in the Arctic Ocean.

2. Materials and Methods

2.1. Water Sampling and Hydrography

Water samples and hydrographic data were obtained onboard the Korean icebreaker R/V Araon every August from 2015 to 2018 in the western Arctic Ocean. The main study regions were from the Bering Strait to an area north of the Chukchi Sea, including north of the East Siberian Sea (NESS) (Figure 1). During the study period, 119 stations were investigated; including 28 stations located in the Chukchi Shelf (CS) region from the Bering Strait to latitude 73°N, and the remaining 91 stations were located north of the Chukchi Sea (NCS) above the 73°N latitude. Additionally, the NCS was divided into high and low chlorophyll-a (Chl-a) regions based on a Chl-a concentration of 0.5 mg m^{-3}, which is the average surface Chl-a concentration in the NCS. In this way, the study area was divided into three regions: CS, low Chl-a of the NCS, NCS(L), and high Chl-a of the NCS, NCS(H), which was mainly located in the NESS. Water samples were retrieved from 5–6 different depths ranging from the surface to 100 m below the surface using 10L Niskin bottles mounted on the conductivity, temperature, and depth rosette system (911 +, SeaBird Electronics). However, the all analysis for this study (hydrographic data, nutrient concentrations, size fractionated Chl-a, and photophysiological data) used only data within the mixed layer to focus on the effects of nutrient limitation on phytoplankton photosynthesis.

Mixed layer depth (MLD), stratification index ($\Delta\sigma_t$), and freshwater content (FWC) were calculated using the temperature and salinity profiles of each station. The MLD was determined as the depth at which the density difference from the surface density was 0.05 kg m^{-3} (Coupel et al., 2015), and $\Delta\sigma_t$ was calculated from the difference in density between the surface and 100 m (Codispoti et al., 2005). To assess freshwater in the upper layer from sea ice melting and river discharge, FWC was defined using the following equation (Coupel et al., 2015; McPhee et al., 2009):

$$\mathrm{FWC} = \int_{z_{lim}}^{0} \left(1 - \left(S(z)/S_{ref}\right)\right) \mathrm{d}z, \tag{1}$$

where $S(z)$ and S_{ref} are the salinity measured at z depths and the reference salinity value, respectively; z_{lim} is the depth at which S equals S_{ref}; and S_{ref} is assigned a value of 31, which is the minimum salinity of the Pacific water flowing through the Bering Strait (Coupel et al., 2015; Woodgate & Aagaard, 2005). Therefore, this reference value excludes water freshening from the Pacific water inflow and allows estimation of the freshening by sea ice melting and river discharge. During the cruise period, photosynthetically active radiation (PAR) was obtained from a quantum sensor (LI-190R, LI-COR) mounted on the ship. The euphotic depth was estimated as the depth at which the PAR was 1% of the surface values (Kirk, 1994). The daily satellite data were obtained from the National Snow and Ice Data Center (https://nsidc.org/) from the scanning multichannel microwave radiometer, the special sensor microwave imager, and the special sensor microwave imager/sounder. The sea ice data were processed using the NASA Team algorithm with a spatial resolution of 25 km^2. Sea ice concentration was set at 15% per pixel, meaning that the sea ice below 15% was classified as open water.

2.2. Size-Fractionated Chl-a and Nutrients Concentration

Chl-a concentration samples (300–500 ml) were filtered through a glass fiber filter (Whatman GF/F) and then extracted in the dark for 24 h with 90% acetone in a conical tube. Chl-a concentrations were measured using a Turner Designs fluorometer (Trilogy) calibrated with a purified Chl-a standard solution (Sigma) following the method described by Parsons et al. (1984). Additionally, for size-fractionated Chl-a measurements (Sieburth et al., 1978), a cascade connection filtration system that included a 20 μm nylon mesh and a nuclepore filter (Whatman International) with a pore size of 2 μm was used to determine the micro ($\geq$20 μm), nano (2–20 μm), and pico Chl-a ($\leq$2 μm). Continuous measurements of the Chl-a concentration were calculated using the relationship between the minimal fluorescence yield and the Chl-a concentration for each station ($p < 0.01$). The photosynthetic pigment was evaluated using high-performance liquid chromatography. The pigment analysis details can be found in Lee et al. (2019). Nutrients were analyzed for nitrite + nitrate ($NO_2 + NO_3$), phosphate (PO_4), and silicate (SiO_2) concentrations. Nutrient concentrations were measured onboard using a four-channel continuous auto-analyzer by applying standard colorimetric methods (QuAAtro; Seal Analytical) according to the manufacturer's instructions (QuAAtro Applications). Nitracline was defined as the shallowest depth with a nitrate gradient of >0.1 μM.

2.3. Phytoplankton Photophysiology Parameters

2.3.1. Continuous Measurement

A new miniaturized fluorescence induction and relaxation (a mini-FIRe) instrument was used in this study to determine the variable fluorescence of phytoplankton (Gorbunov et al., 2020). The principle of operation of this instrument is similar to those of the previous Fast Repetition Rate (FRR) and FIRe systems (Gorbunov & Falkowski, 2004); however, this new instrument exhibits ca. 20 times better sensitivity and signal-to-noise ratio, which is crucial for sampling in oligotrophic waters. The FIRe instrument provides fluorescence saturation within ca. 100 μs (i.e., a single photosynthetic turnover), which is important for the accurate measurement of quantum yields and functional absorption cross-sections (Gorbunov et al., 1999). Near-surface water was collected ship's underway system which supply seawater from ca. 7 m depth and samples were directly measured through a flow system in a constant temperature room maintained in situ sea surface temperature. Since daytime data were affected by high light effects (photoinhibition), only data obtained at nighttime were extracted and used for analysis for regional comparisons.

2.3.2. Discrete Measurement

Seawater samples were collected from the surface mixed layer. Samples were kept at in situ temperature and in low-light conditions (~10 μmol quanta m^{-2} s^{-1}) for approximately 60 min, which was essential for the recovery from photoinhibition and nonphotochemical quenching. The PSII parameters, including the minimal fluorescence yield (F_o; when all reaction centers are open), maximal fluorescence yield (F_m; all reaction centers are closed), photochemical efficiency of PSII (F_v/F_m), and functional absorption cross-section (σ_{PSII}), were measured as described by Kolber et al. (1998). F_v/F_m was calculated using the ratio of variable fluorescence ($F_v = F_m - F_o$) for the maximum fluorescence (F_m). The blank signals were estimated using surface samples after filtering the seawater with a syringe filter (0.2 μm), utilizing the method described by Bibby et al. (2008).

The electron transfer rates (ETR) of the samples obtained from the surface were estimated using a programmable actinic light source mounted on the mini-FIRe. The photosynthetic ETR for each PSII reaction center was calculated using the following equation (Gorbunov et al., 2001):

$$\mathrm{ETR} = E\sigma'_{\mathrm{PSII}}\ (\Delta F'/F_v'), \tag{2}$$

where σ'_{PSII} is the functional absorption cross-section of PSII and $\Delta F'/F_v'$ is the coefficient of photochemical quenching, which is the fraction of open reaction centers at a given level of irradiance. The prime character (′) indicates measurements under programmed irradiance (E). Here, both σ'_{PSII} and $\Delta F'/F_v'$ are functions of irradiance.

When the only cause for non-photochemical quenching of fluorescence is thermal dissipation in the light-harvesting antennae, $\sigma_{PSII}/\sigma'_{PSII} = (F_v/F_m)/(F'_v/F'_m)$ (Suggett et al., 2010) and Equation 2 can be rewritten as follows (Gorbunov et al., 2000):

$$\mathrm{ETR} = E\sigma_{\mathrm{PSII}}\ [(\Delta F'/F_m')/(F_v/F_m)], \tag{3}$$

where $\Delta F'/F_m'$, also denoted as F_q'/F_m' in oceanographic literature, is the only irradiance-dependent variable. The photosynthetic parameters as a function of irradiance can be calculated by the hyperbolic tangent equation (Jassby & Platt, 1976) as follows:

$$\mathrm{ETR(E)} = \mathrm{ETR}^{\max}\tanh(E/E_k), \tag{4}$$

where $\mathrm{ETR}^{\max}$ is the maximum rate achievable at saturating light and E_k is the light saturation parameter. The light utilization efficiency (α) was estimated using $\mathrm{ETR}^{\max}/E_k$. The photosynthetic parameters ($\mathrm{ETR}^{\max}$, E_k, and α) were obtained by applying the experimental data ETR(E) to Equation 4. Additionally, the cross-sections must be measured for the same spectral quality as the ambient irradiance to deduce the photosynthetic rates in absolute units (i.e., electrons per second per reaction center). During our experiments this was the case; blue light (455 nm, with 20 nm half bandwidth) was used for both, excitation light and as actinic light during photosynthesis versus irradiance curves.

2.4. Nutrient Enrichment Experiments

Short-term nutrient enrichment incubations were conducted to assess the extent of nutrient limitation on phytoplankton physiology in 2017–2018. These experiments were carried out at 13 stations, three of which were performed in the CS and the remainder in the NCS (Figure 1b). The samples collected from the mixed layer (ca. 5–10 m) were prefiltered on 100 μm mesh, then placed in 500 ml polycarbonate bottles and incubated for approximately 2–3 days while maintaining in situ temperature and exposing to approximately 50% of the surface irradiance in an incubator located on the deck. This experiment consisted of a control group and three experimental groups with the addition of nitrate (5 μM), phosphate (1 μM), and all nutrients (N, P, Si: 8 μM, Fe: 20 nM). During the incubation, subsamples were taken every day to observe the changes in the

Table 1
Regional Environmental Variables in the Mixed Layer

Region	ST (*N*)	T	S	MLD	Zeu	$\Delta\sigma_t$	FWC	CHL	$NO_2 + NO_3$	PO_4	SiO_2
CS	28	7.06 ± 2.23	31.51 ± 0.96	13 ± 7	26 ± 10	0.95 ± 0.85	3 ± 1	1.69 ± 1.64	1.24 ± 2.42	0.56 ± 0.24	7.72 ± 6.42
NCS(H)	12	−1.21 ± 0.59	30.41 ± 0.66	12 ± 6	23 ± 9	2.29 ± 0.65	8 ± 3	3.22 ± 3.29	0.54 ± 1.3	0.87 ± 0.17	6.65 ± 6.17
NCS(L)	79	−0.84 ± 0.61	27.61 ± 1.54	12 ± 6	55 ± 17	3.94 ± 1.17	15 ± 5	0.11 ± 0.1	0.03 ± 0.12	0.59 ± 0.08	2.05 ± 2.26

Note. Combined all the data from 4 years. Environmental variables (mean and standard deviation) in the Chukchi Shelf (CS) and north of the Chukchi Sea with high, NCS(H), and low, NCS(L), Chl-a concentrations from 2015 to 2018. Temperature (T, °C); salinity (S); mixed layer depth (MLD, m); euphotic depth (Zeu, m); stratification index ($\Delta\sigma_t$, kg m^{-3}); fresh water content (FWC, m); Chl-a concentration (CHL, mg m^{-3}); nitrite + nitrate ($NO_2 + NO_3$, μmol L^{-1}); phosphate (PO_4, μmol L^{-1}); and silicate (SiO_2, μmol L^{-1}). Refer to Figure 1 for location information by region.

phytoplankton photophysiological parameters (F_o, F_v/F_m, σ_{PSII}, and ETR^{max}). Because the phytoplankton community structure did not change during a short-term incubation period, the results of these incubations reflect the responses in phytoplankton physiology. In addition, the incubation period in the NCS was extended to 6–7 days to obtain a full recovery of the photosynthetic capacity in those cold waters, and to observe changes in the phytoplankton community structure. For the latter goal, we analyzed change in three plankton size fraction (≥10, 3–10, and ≤3 μm). The extent of the nutrient limitation was quantified from a relative decrease in photosynthetic parameters (F_v/F_m and ETR^{max}) relative to their control values under nutrient-replete conditions as follows:

$$\Delta F_v/F_m = \left[(F_v/F_m)^{+N} - (F_v/F_m)\right]/(F_v/F_m)^{+N} \times 100\%, \tag{5}$$

$$\Delta ETR^{max} = \left[ETR^{max+N} - ETR^{max}\right]/ETR^{max+N} \times 100\%. \tag{6}$$

Here, F_v/F_m and ETR^{max} are the values recorded in the control samples at the beginning of the incubation experiments and $F_v/{F_m}^{+N}$ and ETR^{max+N} are nutrient-replete values measured at the end of the nutrient enrichment incubations when the photosynthetic rates fully recovered.

2.5. Statistical Analysis

In this study, analysis of variance was used to determine the difference in the distribution of phytoplankton photophysiological properties by region. This analysis was performed using Matlab (R2016a). To understand the relationship between environmental variables, phytoplankton photophysiological properties, and community size structure by region, a principal component analysis was performed, which was calculated using the *factoextra* package (v1.0.6) in R3.6.0 software.

3. Results

3.1. Physical and Chemical Environments

The surface physical, chemical, and biological parameters showed distinct differences between the CS and NCS regions (Table 1). During the cruise, sea ice mainly existed in the NCS and the sea ice concentration was approximately 18 ± 20%. The sea surface temperature and salinity of the CS were in the ranges of 7.06 ± 2.23°C and 31.51 ± 0.96 psu, respectively, which were higher than the NCS ranges of −0.84 ± 0.61°C and 27.61 ± 1.54 psu, respectively. The FWC of the NCS was approximately 2–5 times higher than that of the CS, which resulted in lower sea surface salinity in the NCS. Because the stratification was closely related to the FWC, $\Delta\sigma_t$ at 3.94 ± 1.17 kg m^{-3} was considerably high in the NCS. However, the MLD in the NCS was 12 ± 6 m, which was similar to 13 ± 7 in the CS. The euphotic depth in the NCS was 55 ± 17 m, which was much deeper than 26 ± 10 m in the CS.

Regional differences were also observed in the nutrient distributions, except for phosphate (Table 1, Figure 2). The $NO_2 + NO_3$ concentration in the CS was 1.24 ± 2.42 μM, which was relatively high compared to the concentration of 0.10 ± 0.50 μM in the NCS (Figure 2a), and was sometimes undetectable in the NCS. Similar to the regional distribution of $NO_2 + NO_3$, the SiO_2 concentration in the CS ranged from 7.72 ± 6.42 μM and was approximately 2–3 times higher than the concentration of 2.65 ± 3.41 μM in the NCS (Figure 2c); however, the PO_4 concentration was high (0.56–0.63 μM) and similar in both regions

(Figure 2b), implying that phosphate was not a limiting factor. Meanwhile, interannual differences were observed only in silicate distributions of the NCS ($p < 0.05$).

3.2. Phytoplankton Chl-a Concentration and Community Size Structure Distribution

Continuously measured surface Chl-a also showed a distinct latitudinal gradient and gradually decreased from the Bering Strait to the NCS (Figure 3). During the study period, surface Chl-a concentrations ranged from 0.02 to 12.46 mg m^{-3}. In the CS, the Chl-a concentration was 0.71 ± 1.02 mg m^{-3}, which was relatively higher than in the NCS. Chl-a concentration was generally low at 0.30 ± 0.53 mg m^{-3} in the NCS, and extremely low ($\leq$0.1 mg m^{-3}) in the waters close to the Canada Basin. However, in 2016 the average CS Chl-a concentration was approximately 0.25 mg m^{-3}, which is similar to the NCS concentration of 0.22 ± 0.04 mg m^{-3} (Figure 3b). In 2018, high Chl-a concentrations (0.5–4 mg m^{-3}) were observed in the NCS, mainly in the NESS (Figure 3d). The surface Chl-a concentration in the study area not only showed a distinct regional difference, but also a strong interannual variability was observed in the CS and the NESS.

The average Chl-a concentration and phytoplankton community size structure in the mixed layer taken from station samples and according to region are presented in Figure 4. Chl-a concentration in the CS was 1.69 ± 1.64 mg m^{-3}, which is considerably higher than the 0.51 ± 1.60 mg m^{-3} concentration in the NCS and shows a similar trend to the results of Chl-a concentration continuous measurement (Table 1). Considering the phytoplankton community size structure over the last 4 years, the micro-sized phytoplankton community size structure in the CS prevailed at 52 ± 24%, whereas the nano-sized and pico-sized phytoplankton community size structures were dominant at 35 ± 16% and 30 ± 22%, respectively, in the NCS. In particular, the NCS showed a high Chl-a concentration in 2017–2018 (3.22 ± 3.29 mg m^{-3}) and the micro-sized phytoplankton community size structure was responsible for more than 80% (Figure 4d). The phytoplankton community size structure and the Chl-a concentration seem to vary regionally.

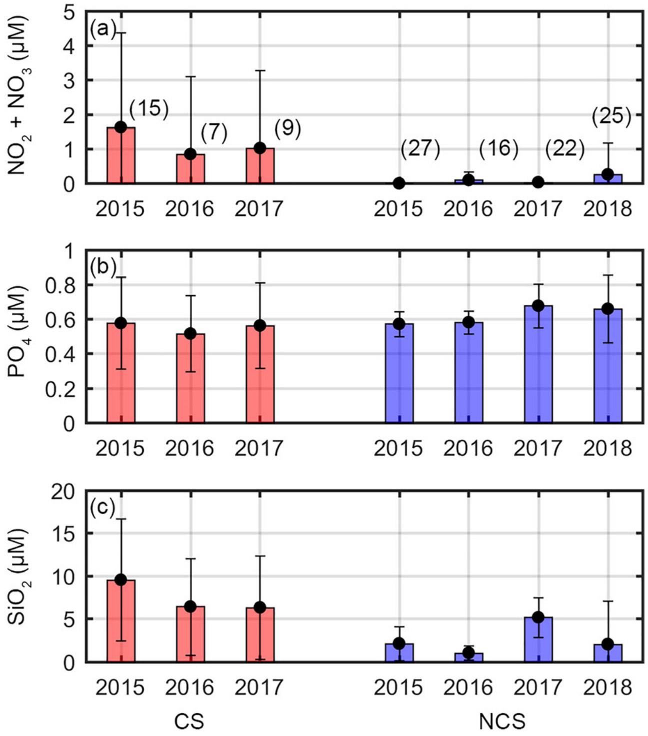

Figure 2. Regional average and standard deviation of nutrient concentrations in the mixed layer for each year (a) nitrite + nitrate concentration ($NO_2 + NO_3$), (b) phosphate concentration (PO_4), and (c) silicate concentration (SiO_2). The study regions are the Chukchi Shelf (CS) and north of the Chukchi Sea (NCS). Numbers in parentheses represent the sample numbers in each year and region.

3.3. Regional Differences in Photochemical Efficiency, Maximum Electron Transfer Rate, and P-E Parameters

Continuous measurement of F_v/F_m in the near-surface showed a diel cycle and latitudinal gradient (Figure 5). In general, F_v/F_m had maximum values at night and decreased during the day due to photoinhibition. For this portion of the study, only the nighttime data were extracted and used for regional comparison. In the CS, the F_v/F_m was a maximum of 0.61, and it was higher than that in the NCS on average (0.46 ± 0.05 and 0.28 ± 0.09, respectively, $p < 0.05$). Meanwhile, F_v/F_m in the CS showed low values (0.39 ± 0.06) in 2016 (Figure 5b), and F_v/F_m in the NESS had relatively high values (average of 0.44 ± 0.05) with a maximum of 0.55 in 2018 (Figure 5d).

The regional distribution of F_v/F_m, σ_{PSII}, and P-E parameters are shown in Figure 6 and Table 2 using station data. The NCS photophysiological data were obtained by classifying the region based on the Chl-a concentration (0.5 mg m^{-3}). The CS F_v/F_m was higher than that of the NCS(L) (0.56 ± 0.03 and 0.46 ± 0.09, respectively) and the NCS(H), primarily the NESS, had a similar F_v/F_m value (0.54 ± 0.07) as that of the CS (Figure 6b). Although σ_{PSII} in the NCS(L) ranged from 200–900 × 10^{-20} m^{-2} $photon^{-1}$, the average value was approximately 490 × 10^{-20} m^{-2} $photon^{-1}$, similar to that in other regions (Figure 6c). For ETR^{max}, the values, presented in decreasing order, were CS (140 ± 63 e^{-1} s^{-1} RC^{-1}), NCS(H) (108 ± 20 e^{-1} s^{-1} RC^{-1}), and NCS(L) (83 ± 34 e^{-1} s^{-1} RC^{-1}) (Figure 6d). E_k in the NCS was much lower than in the CS (<50 and 134 ± 87 μmol photons m^{-2} s^{-1}, respectively) (Figure 6e). However, α in the CS was

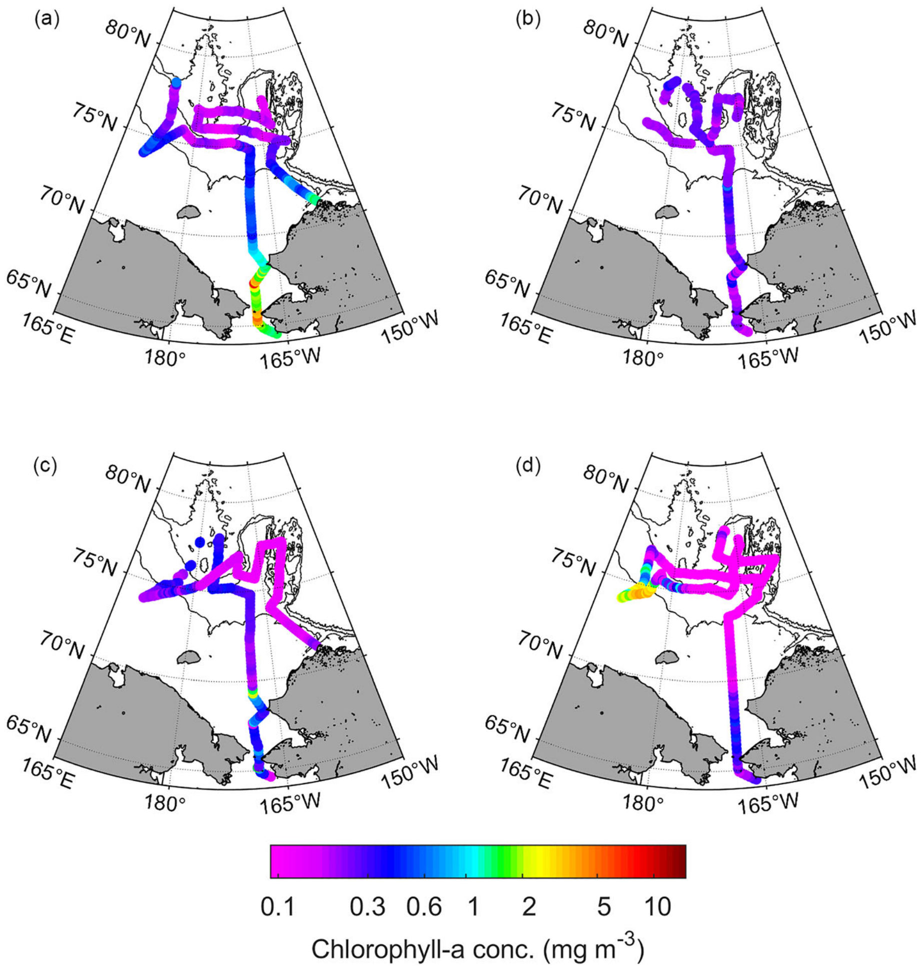

Figure 3. Chl-a concentrations on the surface measured underway according to the ship track in each year (a) 2015, (b) 2016, (c) 2017, and (d) 2018. Black lines indicate the 100-, 1,000-, and 2000-m isobaths.

relatively lower than that of the NCS (1.63 ± 1.12 and 2.53 ± 1.12 μmol electrons (μmol photons)$^{-1}$, respectively) (Figure 6f). Based on these results, except for σ_{PSII}, the photophysiological characteristics represented different distributions by region.

The regional distributions of photophysiological parameters, after being classified according to the phytoplankton community size structure, are presented in Figure 7, which shows that the large group has ≥50% of the micro-sized phytoplankton community, while the small group has ≥50% of the nano-sized or pico-sized phytoplankton community. In the CS, the F_v/F_m of the large group was approximately 12% higher than that of the small group (0.57 ± 0.03 and 0.51 ± 0.03, respectively) (Figure 7a). In contrast, the F_v/F_m of the small group in the NCS(L) was 18% higher than that in the large group (0.47 ± 0.08 and 0.40 ± 0.12, respectively) (Figure 7c). Additionally, the F_v/F_m of the large group in the NCS(H) was comparable to that of the large group in the CS (Figure 7b). However, no significant difference in the σ_{PSII} was observed in the groups of each region. Similar to the distribution of F_v/F_m, in the large group of the CS, ETR$^{\mathrm{max}}$ and α were relatively larger than those in the small group (ETR$^{\mathrm{max}}$: 165 ± 73 and 93 ± 2 e^{-1} s^{-1} RC^{-1}, respectively; α: 2.14 ± 1.03 and 0.80 ± 0.23 μmol electrons [μmol photons]$^{-1}$, respectively) (Figure 7d). E_k had no distinction by community size in the CS (112 ± 76 μmol photons m^{-2} s^{-1}), whereas in the NCS, ETR$^{\mathrm{max}}$ and E_k were 88 ± 34 e^{-1} s^{-1} RC^{-1} and 40 ± 28 μmol photons m^{-2} s^{-1}, respectively, and the α value was very high (≥2.5 μmol electrons [μmol photons]$^{-1}$) (Figures 7d–7f). Although ETR$^{\mathrm{max}}$ and α showed differences between groups in the CS, the P-E parameters had similar values in the NCS.

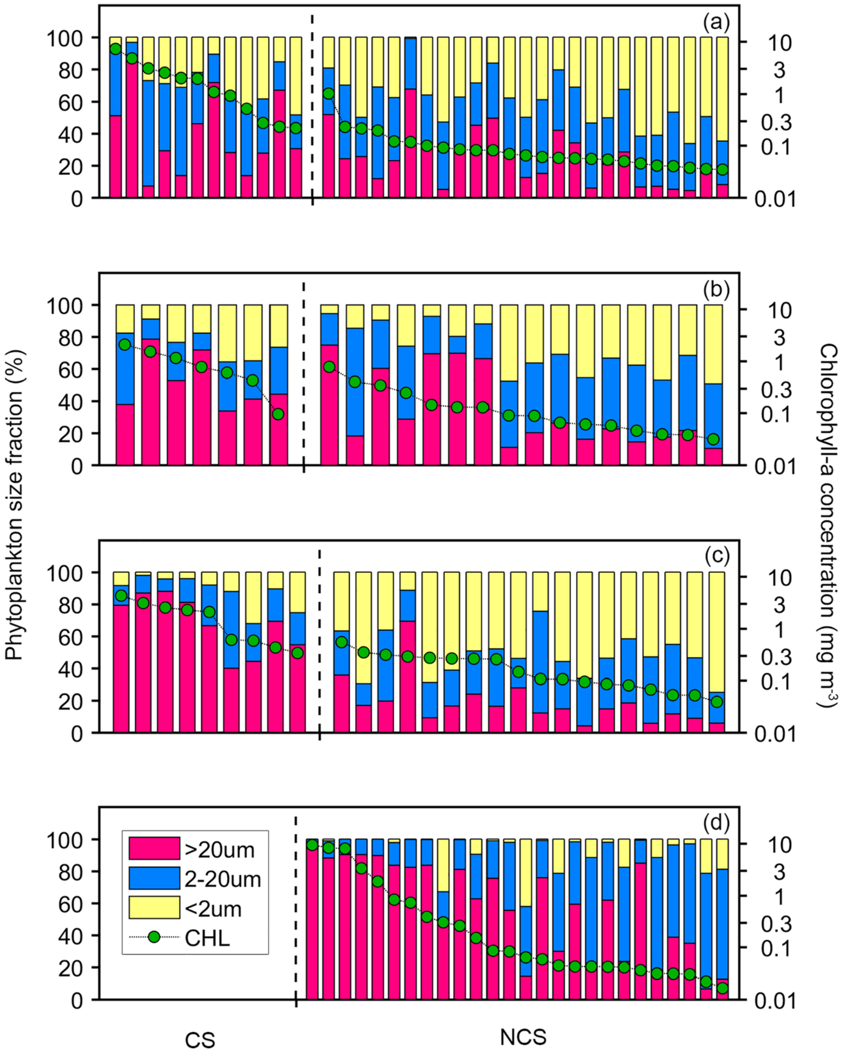

Figure 4. Regional distribution of phytoplankton size fraction (%) and Chl-a concentration (mg m^{-3}) in the mixed layer in each year (a) 2015, (b) 2016, (c) 2017, and (d) 2018. The regions are divided into the Chukchi Shelf (CS) and the north of Chukchi Sea (NCS) denoted by the black dashed line.

3.4. Photophysiological Responses of Phytoplankton to Nutrient Enrichment

Phosphate additions did not produce any significant response in all incubations, clearly suggesting that phosphate was abundant and did not limit phytoplankton photosynthesis or growth. Nitrate addition induced a significant increase in photosynthetic capacity in most experiments and this response was the same as that for the full nutrient addition. Below, we show results for nitrogen enrichment experiments, including both short-term and long-term incubations (Figure 8 and Table 3). Nitrate addition increased the F_v/F_m, ETR^{max}, and Chl-a concentration in the samples in most cases. In three experiments performed in the CS, Experiment 01 (E01) did not show the phytoplankton photophysiological responses to nitrate enrichment, suggesting that this area was nutrient replete. F_v/F_m increased by 7% without increasing the ETR^{max} and Chl-a concentration while in Experiment 02 (E02), and in Experiment 03 (E03) only the ETR^{max} and Chl-a concentration increased by approximately 20% without increasing $\Delta F_v/F_m$. However, there were no statistically significant changes in these variables. σ_{PSII} did not change significantly in any of the CS tests (Figure 8c).

Meanwhile, in the short-term incubation experiments in the NCS, the addition of nitrate enhanced the F_v/F_m and ETR^{max} by 10 ± 9% and 15 ± 11%, respectively, and at the same time, increased the Chl-a concentration by 26 ± 16% ($p < 0.05$). In addition, the F_v/F_m and ETR^{max} increased by 12 ± 9% and 40 ± 17%,

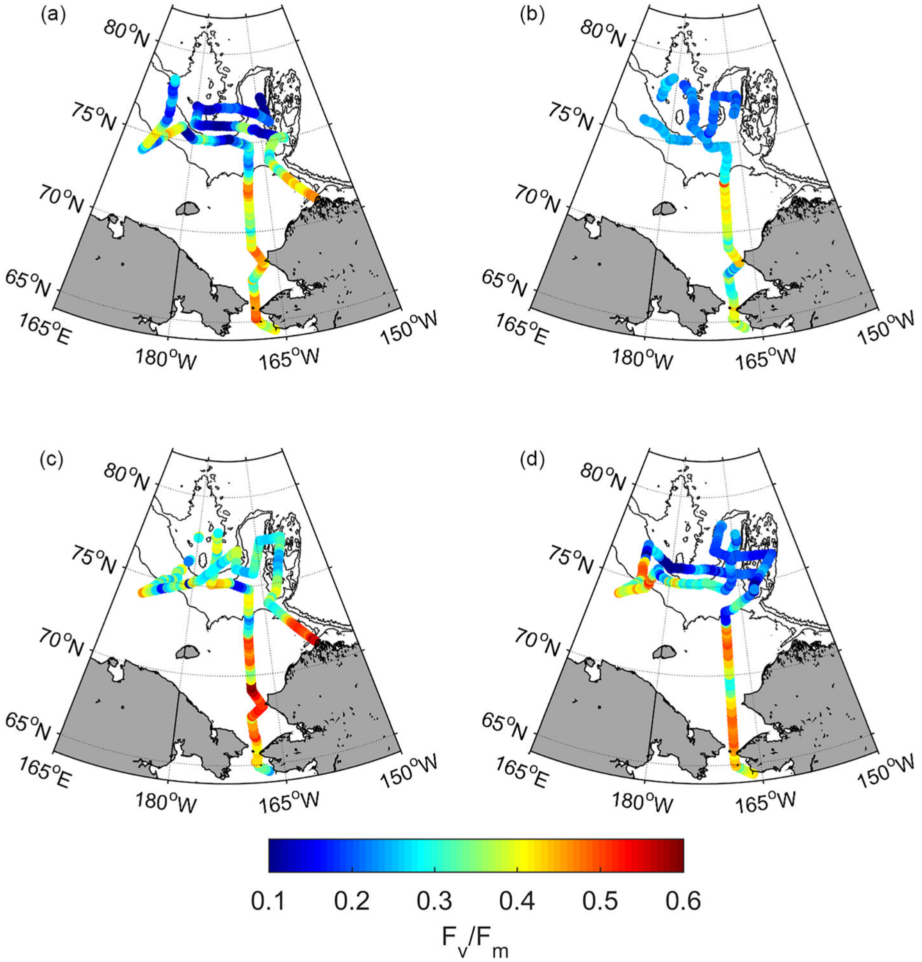

Figure 5. Photosynthetic efficiency (F_v/F_m) at the surface measured underway according to the ship track in each year (a) 2015, (b) 2016, (c) 2017, and (d) 2018. Black lines indicate the 100-, 1,000-, and 2000-m isobaths.

respectively, and the Chl-a concentration increased by 77 ± 17% during the long-term incubation period ($p < 0.05$). During the short-term and long-term incubation periods, σ_{PSII} decreased slightly but did not show a clear increase or decrease in the NCS (Figure 8c). Because of the regional experiments performed with the addition of nitrate, the scale of change of the photophysiological variables and Chl-a concentration in the NCS was larger than that in the CS.

4. Discussion

4.1. Nitrate Availability Governs the Phytoplankton Physiological Status

Nitrogen is a major limiting factor for phytoplankton growth in the Arctic Ocean (Danielson et al., 2017; Lowry et al., 2015; Tremblay et al., 2006). In this study, the CS had sufficient nitrogen supply to the surface in the summer owing to the influence of the Bering Strait summer water (relatively cold and saline Pacific-origin water), with the Atlantic water (nutrient-rich) originating from upwellings from Barrow and Herald Canyons (Pickart et al., 2010; Pisareva et al., 2019; Wang et al., 2005). In the NCS, the large supply of freshwater occurs at the time when the sea ice retreats in the summer, causing a deep nitracline along with a strengthened stratification of the water column, which inhibits nitrogen supply from the bottom to the surface (Coupel et al., 2015; Yun et al., 2016). Likewise, our study showed a marked difference in the surface nutrient distribution between the two regions in the summer (Figure 2). In particular, the surface nitrate in the NCS was virtually exhausted (≤0.1 μM).

The average CS surface Chl-a concentration was more than three times higher than that in the NCS, and the phytoplankton community size structure was also distinguished mainly by micro-sized communities in the

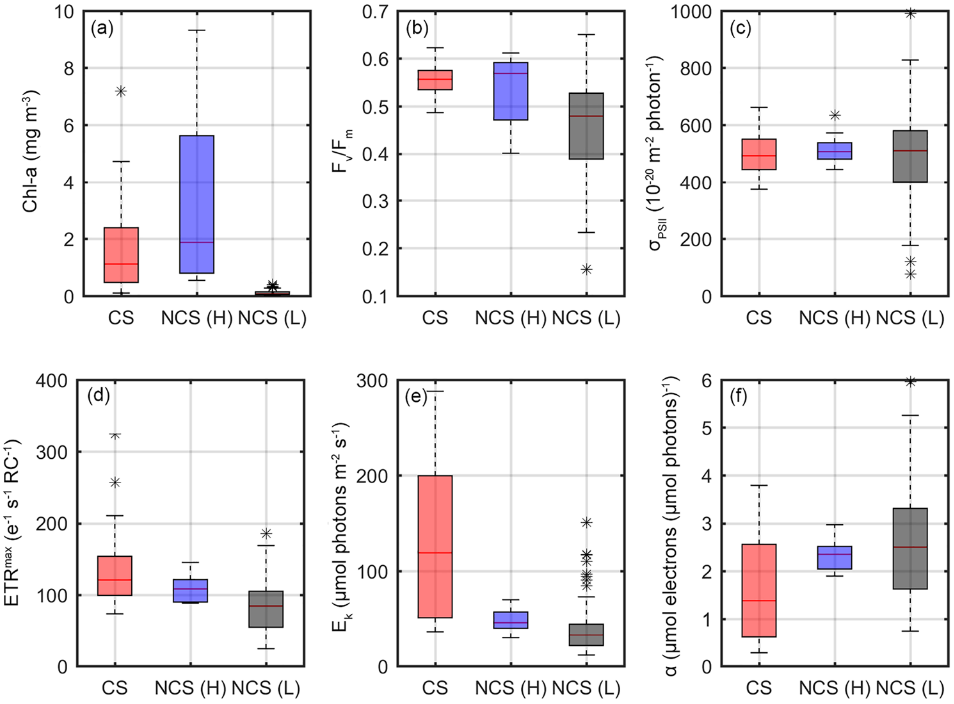

Figure 6. Box plots of photophysiological characteristics in the mixed layer in the three regions. The regions consist of the Chukchi Shelf (CS) and north of the Chukchi Sea with high, NCS(H) and low, NCS(L), Chl-a concentrations. (a) Chl-a concentration (Chl-a; mg m^{-3}), (b) Photochemical efficiency (F_v/F_m), (c) Functional absorption cross-section (σ_{PSII}), (d) maximum electron transfer rate (ETR^{max}), (e) light saturation for photosynthesis (E_k), and (f) light utilization efficiency (α).

CS and nano-sized and pico-sized communities in the NCS (Figures 3 and 4). The spatial distributions of nutrient concentration, Chl-a concentration, and community size structures in the upper layer of these two regions showed distinct differences, which was similar to the findings of previous studies (Coupel et al., 2012, 2015; Fujiwara et al., 2016). It was expected that regional nitrate availability would eventually lead to differences in the Chl-a concentration and phytoplankton community size structure between these two regions.

Phytoplankton photophysiological parameters also differed significantly between the two regions. Phytoplankton photochemical efficiency in the surface gradually decreased from CS to NCS (Figure 5), indicating an increase in nutrient stress (Behrenfeld & Kolber, 1999; Kolber et al., 1994; Lin et al., 2016). The average F_v/F_m in the NCS mixed layer was 0.46, which was approximately 22% lower than that in the CS ($p < 0.05$, Table 2, Figure 6b). Moreover, compared with the theoretical maximum value (0.65) determined by Kolber and Falkowski (1993), approximately 40% of the PSII reaction centers appear to have been inactive. Zhu et al. (2019) also reported that the F_v/F_m in the Chukchi Borderland was approximately 24% lower

Table 2
Regional Phytoplankton Photophysiology Variables in the Mixed Layer

Region	ST (*N*)	Chl-a	F_v/F_m	σ_{PSII}	ETR^{max}	E_k	α
CS	28	1.69 ± 1.64	0.56 ± 0.03	493 ± 72	140 ± 63	134 ± 87	1.63 ± 1.12
NCS(H)	12	3.23 ± 3.29	0.54 ± 0.07	516 ± 51	108 ± 20	48 ± 13	2.33 ± 0.35
NCS(L)	79	0.11 ± 0.10	0.46 ± 0.09	499 ± 170	83 ± 34	41 ± 30	2.56 ± 1.19

Note. Phytoplankton photophysiological variables (mean and standard deviation) in the mixed layer in the Chukchi Shelf (CS) and north of the Chukchi Sea with high, NCS(H), and low, NCS(L), concentrations from 2015 to 2018. Chl-a concentration (Chl-a); Maximum photochemical efficiency (F_v/F_m); functional absorption cross-section (σ_{PSII}, 10^{-20} m^2 $photons^{-1}$); maximum electron transfer rate (ETR^{max}, e^{-1} s^{-1} RC^{-1}); minimum saturating irradiance (E_k, μmol photons m^{-2} s^{-1}); and light utilization efficiency (α, μmol electrons [μmol $photons]^{-1}$).

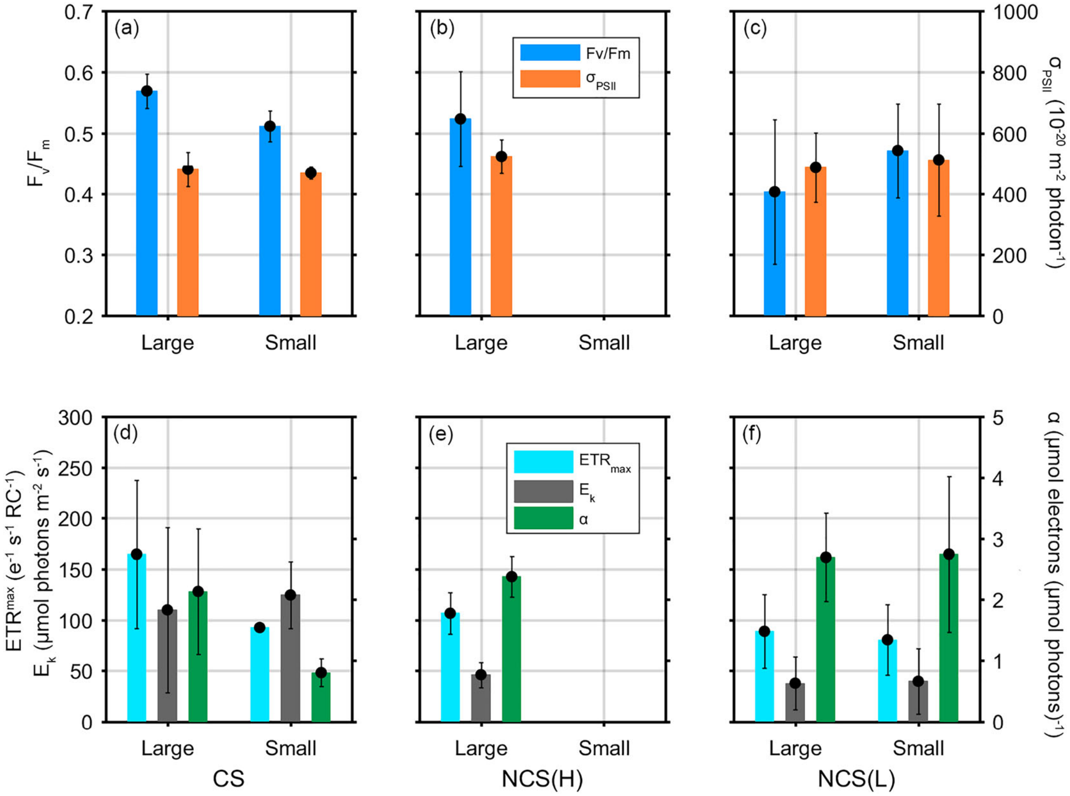

Figure 7. Distribution of photophysiological characteristics of large and small groups by region consisting of the Chukchi Shelf (CS) and the Northern Chukchi Sea with high, NCS(H), and low, NCS(L), Chl-a concentrations in the mixed layer. The large group is dominated by a micro-sized phytoplankton community (>50%), and the small group is dominated by nano-sized and pico-sized phytoplankton communities (>50%). All available data during the 4 years were used. The number of stations for large and small groups is 14 and 2 in the CS, 9 and 0 in the NCS(H), and 15 and 27 in the NCS(L), respectively. The photophysiological parameters of each panel correspond to those in Figure 6.

than in the CS waters, which was similar to the results of this study. Meanwhile, the F_v/F_m observed off the coast of the Arctic Ocean is known to remain high (≥0.50) throughout the year, except immediately after the spring bloom (Aardema et al., 2019; Kulk et al., 2018; McMinn & Hegseth, 2004; Mills et al., 2018; Mosharov et al., 2019). This study also showed high phytoplankton F_v/F_m values (0.56) in Arctic coastal waters in the summer, indicating the lack of nutrient stress. The $\mathrm{ETR}^{\mathrm{max}}$ observed in the NCS was approximately 30% lower than that observed in the CS (Figure 6d). As expected, F_v/F_m and $\mathrm{ETR}^{\mathrm{max}}$ were relatively low in the NCS; however, the decline in $\mathrm{ETR}^{\mathrm{max}}$ was slightly larger than that in F_v/F_m.

On the other hand, exceptionally high F_v/F_m values (~0.52) and an $\mathrm{ETR}^{\mathrm{max}}$ similar to that of the CS were observed in the NCS(H) in 2017–2018 (Figures 6b and 6d). At that time, although the surface nitrate concentration was not high (ca. 0.5 μM), the average Chl-a concentration was relatively high (≥3 mg m^{-3}) compared to that in the NCS (≤0.5 mg m^{-3}). These results imply that the temporary nitrate supply occurred in this region in the summers of 2017 and 2018, causing an increase in the phytoplankton biomass. This study further compared the vertical distributions of $NO_2 + NO_3$ in the CS, NCS(L), and NCS(H) in 2017–2018 (Figure 9). The nitracline in the CS and NCS(H) was formed at a shallow depth rather than the MLD (nitracline: 6–24 m, MLD: 5–20 m), indicating that the nitrate supply to the surface was relatively good. In contrast, in the NCS(L), the nitracline was formed deeper than the MLD, which would have limited nitrate supply to the surface (nitracline: 23–43 m, MLD: 5–18 m). Therefore, nitrate availability would have played an important role in determining phytoplankton photophysiology in the Arctic Ocean. Considering the F_v/F_m and $\mathrm{ETR}^{\mathrm{max}}$ of these two regions observed over the past 4 years, it was determined that the phytoplankton photophysiology was hindered by approximately 20%–30% in the nitrate-depleted NCS. In particular, the decrease in the maximum photosynthetic rates (ca. $\mathrm{ETR}^{\mathrm{max}}$) was more significant than that in F_v/F_m.

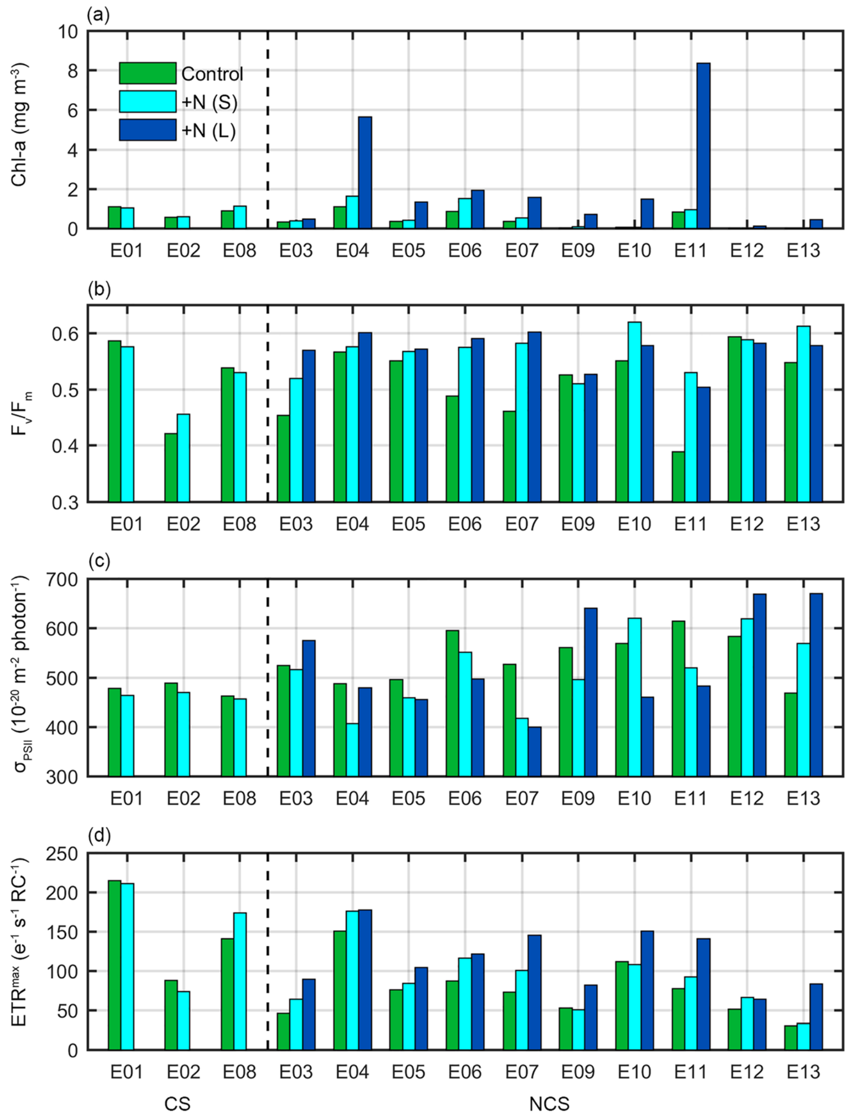

Figure 8. Changes in photophysiological characteristics after short-term (2–3 days) and long-term (6–7 days) experiments with nitrate addition in the Chukchi shelf (CS) and north of the Chukchi Sea (NCS). Experiment 01 (E01) to 07 (E07) was conducted in 2017, and Experiment 08 (E08) to 13 (E13) was performed in 2018. (a) Chl-a concentration (mg m^{-3}), (b) photochemical efficiency (F_v/F_m), (c) functional absorption cross-section (σ_{PSII}), and (d) maximum electron transfer rate (ETR^{max}). In each experiment, the green bar represents the control samples, and the cyan and blue bars represent the nitrate addition samples in short-term and long-term incubation, respectively. The black dashed line represents the regional classifications.

4.2. Other Environmental Factors Affecting Phytoplankton Physiology

In addition to nitrate availability, other environmental factors may also affect the phytoplankton photophysiological distribution in the Arctic Ocean. We utilized a principal component analysis to elucidate the relationship between regional environmental variables and phytoplankton-related variables (e.g., Chl-a concentration, photophysiological properties, and community size structure). In the first principal component (PC1: 33%), nutrients, F_v/F_m, and ETR^{max} were negatively correlated with FWC, $\Delta\sigma_t$, and nitracline, associated with the inhibition of nitrate supply to the surface, suggesting that the surface nitrate status plays an important role in the phytoplankton photophysiology between the CS, NCS(H), and NCS(L) (Figure 10). Phytoplankton had relatively high F_v/F_m and ETR^{max} in the CS where nitrate availability was good, and Chl-a concentration was high. The photophysiological properties of phytoplankton was evaluated to be low in the NCS(L) where surface nitrate was depleted, accordingly, very low Chl-a concentration was

Table 3
Measurements of Nitrate Enrichment Incubations by Region

Region	Year	Control								+Nitrate							
		CHL		F_v/F_m		ETR^{max}		$f_{\geq 10\ um}$		CHL		F_v/F_m		ETR^{max}		$f_{\geq 10\ um}$	
CS	2017	1.09		0.59		215		ND		1.04		0.58		211		ND	
		0.57		0.42		88		ND		0.60		0.46		74		ND	
	2018	0.90		0.54		141		ND		1.13		0.53		174		ND	
NCS	2017	0.31	0.28	0.45	0.45	46	45	ND	0	0.40	0.49	0.52	0.57	64	89	ND	1
		1.11	1.61	0.57	0.52	151	133	ND	66	1.62	5.65	0.58	0.60	176	178	ND	83
		0.35	0.32	0.55	0.55	76	59	ND	0	0.41	1.33	0.57	0.57	84	105	ND	70
		0.86	0.68	0.49	0.53	87	85	ND	0	1.53	1.92	0.57	0.59	116	121	ND	68
		0.34	0.30	0.46	0.51	73	127	ND	42	0.55	1.57	0.58	0.60	100	146	ND	71
	2018	0.04	0.08	0.53	0.48	53	41	ND	0	0.07	0.72	0.51	0.53	51	82	ND	15
		0.06	0.07	0.55	0.53	112	48	ND	45	0.06	1.50	0.62	0.58	108	150	ND	74
		0.83	0.32	0.39	0.35	77	59	ND	80	0.97	8.36	0.53	0.50	93	141	ND	93
		0.01	0.02	0.59	0.54	52	48	ND	0	0.01	0.12	0.59	0.58	66	64	ND	0
		0.01	0.14	0.55	0.59	31	52	ND	14	0.01	0.46	0.61	0.58	34	84	ND	16

Note. Regional photophysiological variables and size fraction (≥10 μm) for the natural phytoplankton community incubated without additional nutrients (control) and additional nitrate (+Nitrate) in the Chukchi Shelf (CS, short-term incubation) and north of the Chukchi Sea (NCS, short-term and long-term incubation). Chl-a concentration (CHL, mg m^{-3}); maximum photochemical efficiency (F_v/F_m); maximum electron transfer rate (ETR^{max}, e^{-1} s^{-1} RC^{-1}); the ratio of ≥10 μm phytoplankton community size structure ($f_{\geq 10\ \mu m}$; %); and ND is no data.

recorded on average. The results of NCS(H) indicated that the new supply of nutrients to the surface of the Arctic Ocean not only increased the photophysiological properties and biomass of phytoplankton but also led to a change in phytoplankton community size. In addition, most of the micro-sized phytoplankton in the CS and NCS(H) were determined to be diatom-dominated owing to a very high fucoxanthin

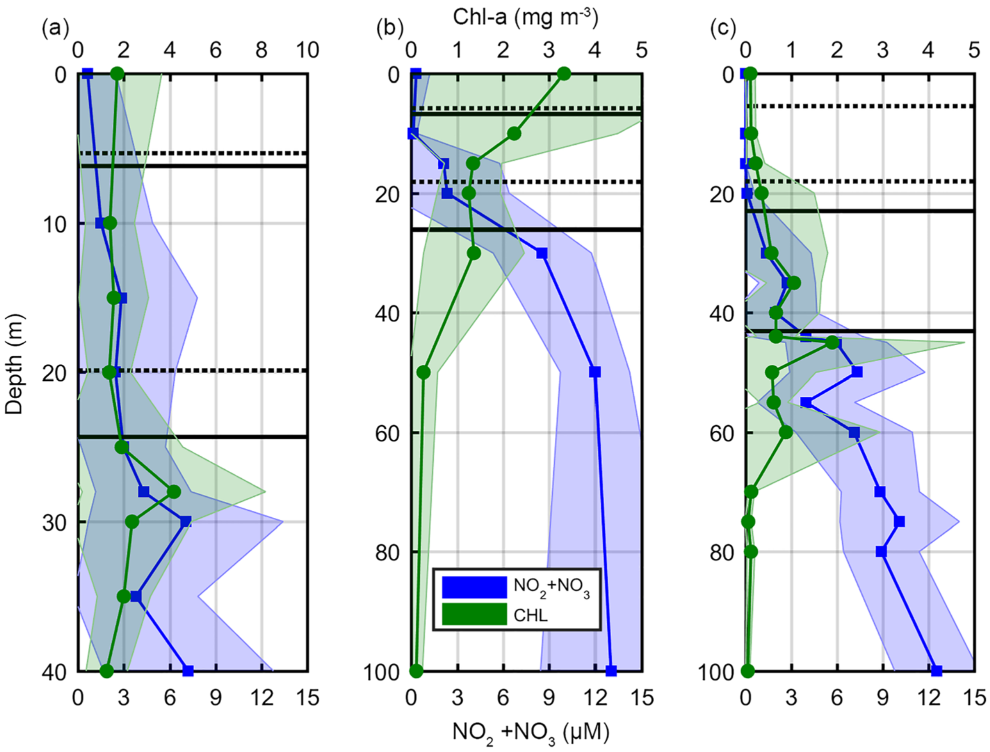

Figure 9. Vertical profiles of nitrite + nitrate ($NO_2 + NO_3$) and Chl-a by region. The regions consist of (a) the Chukchi Shelf, (b) the north of the Chuchi Sea with high Chl-a concentration, and (c) north of Chukchi Sea with low Chl-a concentration. The solid line and shading represent average and standard deviation values of $NO_2 + NO_3$ and Chl-a concentrations by depth, respectively. Two horizontal black solids and dotted lines on each panel represent the range that includes mean ± standard deviation of nitracline and the MLD, respectively.

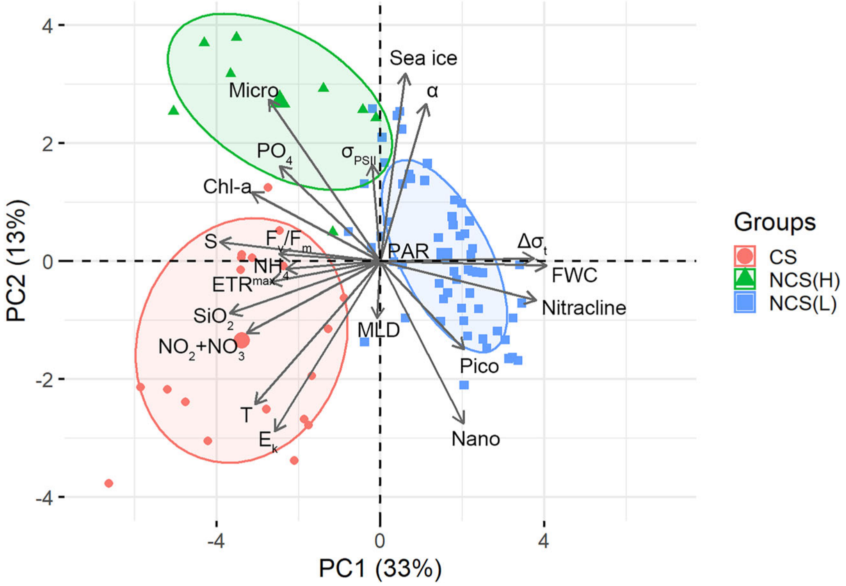

Figure 10. Biplot of the first and second principal components (PC1: 33%, PC2: 13%) between the environmental variables and phytoplankton photophysiological parameters grouped by regions of the Chukchi Shelf (CS) and north of the Chukchi Sea with high, NCS(H), and low, NCS(L), Chl-a concentrations. Terms and abbreviations: temperature (T); salinity (S); photosynthetically active radiation (PAR); mixed layer depth (MLD); nitracline; freshwater content (FWC); stratification index ($\Delta\sigma_t$); sea ice; Chl-a concentration (Chl-a); size fraction (micro, nano, pico, %); photochemical efficiency (F_v/F_m); functional absorption cross-section (σ_{PSII}); maximum electron transfer rate (ETR^{max}); light saturation for photosynthesis (E_k); light utilization efficiency (α); nitrite + nitrate ($NO_2 + NO_3$); phosphate (PO_4); and silicate (SiO_2).

concentration (Figure S1 in the supporting information). In the NCS(L), nano-sized and pico-sized phytoplankton communities were mainly small-sized flagellates containing fucoxanthin because the proportion of the fucoxanthin and chlorophyll-b concentration was high (Figure S1; see also Coupel et al., 2012, 2015; Fujiwara et al., 2016; Lee et al., 2019). On the other hand, the F_v/F_m of the small-sized phytoplankton communities was relatively higher than that of the large-sized phytoplankton communities in the NCS(L) (Figure 7c), which seemed to be caused by the high nutrient uptake rate of the small-sized phytoplankton by the large surface-to-volume ratio (Lindemann et al., 2016; Raven, 1998). Therefore, the results of the principal component analysis suggested that the environmental variables related to nitrate availability were major factors controlling the regional distribution of the phytoplankton biomass, photophysiology, and community size structure.

In PC2 (13%), E_k showed a negative correlation with sea ice, α, and σ_{PSII}, which probably indicates photoadaptation of phytoplankton by light history. In particular, α and σ_{PSII} have a positive correlation with sea ice, representing that phytoplankton increases the light absorption rate in waters with low light under sea ice (Furuya et al., 1998). Eukaryotes generally tend to increase σ_{PSII} under nutrient-limited conditions (Kolber et al., 1988). However, this study did not show a significant difference in σ_{PSII} by region or community size structure (Figures 6c and 7). The distribution of σ_{PSII} did not exhibit a specific trend because it was influenced by various factors such as phytoplankton community structure, cell size, and pigment concentration (Geider et al., 1986; Moore et al., 2005; Suggett et al., 2004, 2009). In terms of light history, the daily average CS PAR was more than 50% higher than that of the NCS (25 ± 13 and 16 ± 6 E m^{-2} d^{-1}, respectively), and regional differences in E_k and α were also clearly observed. Unlike the CS, E_k in the NCS was less than 50 μmol m^{-2} s^{-1}, indicating that the phytoplankton in this region have adapted to very low light (Figures 6e and 6f). However, given that the average PAR in the mixed layer was mostly higher than the E_k in the summer, phytoplankton in the NCS was unlikely to be significantly affected by light limitations (Figure S2). On the other hand, nitrate limitation may interfere with the ability of phytoplankton to adapt to high light; therefore, Arctic phytoplankton remain adapted to low light and would have modified light absorption to protect against photoinhibition (Alou-Font et al., 2016; Lewis et al., 2019). In other words, light history

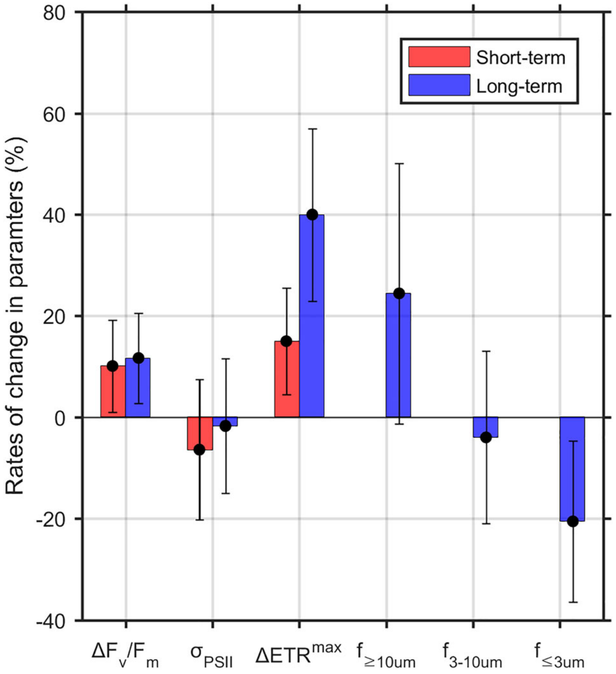

Figure 11. Changes in photophysiological parameters and phytoplankton community size after short-term (2–3 days) and long-term incubation (6–7 days) north of the Chukchi Sea. Photophysiological parameters include photochemical efficiency ($\Delta F_v/F_m$), functional absorption cross-section (σ_{PSII}), and maximum electron transfer rate (ΔETR^{max}). Phytoplankton community size consisted of ≥10 μm, 3–10 μm, and ≤3 μm.

and light-related environmental conditions (e.g., sea ice) controlled the photoadaptation mechanism of phytoplankton.

Meanwhile, phytoplankton in the NCS(H) showed high photosynthetic efficiencies and a low light-adapted status, which may be related to the transient nitrate supply and low light conditions explained earlier. In the NCS(H), when moderate nitrogen stress was expected, the E_k values were slightly higher than in the NCS(L). The transient increase in ambient nitrate concentrations did not seem to significantly affect the E_k or α of the phytoplankton that were already adapted to low light. In conclusion, this study confirmed that the phytoplankton photophysiological properties in each region were influenced by the combination of nitrate availability and light history.

4.3. Phytoplankton Photophysiological Responses to Nitrogen Limitation

On-deck nutrient enrichment experiments were conducted at several locations to quantify the effects of nitrogen stress on F_v/F_m and ETR^{max} in the phytoplankton in the Arctic Ocean (Figure 8). The short-term incubations were designed to stimulate only the physiological responses without a change in community composition (Park et al., 2017). Nitrogen enrichment produced the same effects as full nutrient enrichment, and phosphate addition had no effect at all. These results clearly suggest that nitrogen was the sole limiting nutrient. In the three experiments conducted in the CS, there were no significant responses in photophysiological properties to the addition of nitrate. However, in the NCS experiments, F_v/F_m and ETR^{max} increased by 10 ± 9% and 15 ± 11%, respectively ($p < 0.05$). The functional cross-section of PSII in our incubations exhibited various responses to the addition of nitrate (Figure 8c). In particular, no change or increase in the σ_{PSII} implied that phytoplankton consumed energy to repair damaged reaction centers or synthesize new reaction centers (Behrenfeld et al., 1998; Falkowski & Raven, 2007; Mills et al., 2018). ΔETR^{max} was much larger than $\Delta F_v/F_m$, suggesting that phytoplankton in the NCS could be hampered more by the production of photosynthetic enzymes and proteins (Kolber et al., 1988; Mills et al., 2018). This significant increase in ETR^{max} with a small or no increase in F_v/F_m is a typical biophysical signature of nitrogen stress in phytoplankton (Gorbunov & Falkowski, 2020).

Long-term incubations were conducted in the low-temperature waters of the NCS to promote full recovery of the phytoplankton photosynthetic capacity. These long-term incubations revealed that F_v/F_m and ETR^{max} increased by 12 ± 9% and 40 ± 17%, respectively, and the fraction of large (≥10 μm) phytoplankton increased by approximately 25% compared to the beginning of culture sample (Figure 11). In turn, larger cells fraction exhibited increased photosynthetic capacity (Kulk et al., 2018; Mills et al., 2018). Mills et al. (2018) reported an increase in the large-sized diatom biomass in response to nitrate enrichment in the Chukchi Sea. The observed ETR^{max} reduction under nitrogen stress (ca. 40%) in our study was very large, indicating severe impairment of growth rates and net primary production (Gorbunov & Falkowski, 2020). Based on the results from laboratory experiments (Gorbunov & Falkowski, 2020), a ΔETR^{max} of approximately 40% suggests a very strong (ca. 80%) reduction in the net primary production rate under nitrogen stress in the NCS.

Based on the results of this study, we have explained difference in the distributions of phytoplankton biomass and photophysiology in two regions of the Arctic Ocean, where nitrate availability was markedly different. Our results revealed that the paucity of nitrogen has a very strong effect on photosynthetic rates in this region in the summer. Severe nitrogen limitation reduced phytoplankton photosynthetic capacity, growth, and net primary production; thereby suppressing the growth of larger plankton to a greater extent. Climate changes in the marine environment of the Arctic Ocean would greatly alter the nitrogen distribution by region. For example, strengthened stratification by freshwater may impair the nutrient supply to the upper layer (Coupel et al., 2015; Yun et al., 2016) or wind mixing and shelf break upwelling could deliver new nutrients (Lewis et al., 2020). Therefore, the primary production and phytoplankton community structure are expected to change according to the supply mechanism of nutrients in each region of the Arctic Ocean. Our results have important implications for understanding how climate-driven variation of nitrogen flux in the Arctic Ocean would affect phytoplankton communities and primary production.

Data Availability Statement

The sea ice concentration data were obtained from the National Snow and Ice Data Center (https://nsidc.org/). The phytoplankton size-fractionated Chl-a and pigments data are available through Lee et al. (2019). Except for photophysiology data, all data used in this study are publicly available at the Korea Arctic Ocean data System (https://kaos.kopri.re.kr/uat/uia/actionAnonymousLogin.do). Photophysiology data are available at the Korea Polar Data Center (https://kpdc.kopri.re.kr).

Acknowledgments

This research was a part of the project titled "Korea-Arctic Ocean Observing System (K-AOOS)", the Korea Polar Research Institute (KOPRI) 20160245, funded by the Ministry of Oceans and Fisheries (MOF), Korea. MYG was in part funded by NASA Ocean Biology and Biogeochemistry Program (grants NNX16AT54G and 80NSSC18K1416). We thank the captain and the crew of the R/V Araon for assistance with field data collection, Kevin Wyman for suggestions on the manuscript, and the editor and anonymous reviewers for constructive comments.

References

Aardema, H. M., Rijkeboer, M., Lefebvre, A., Veen, A., & Kromkamp, J. C. (2019). High-resolution underway measurements of phytoplankton photosynthesis and abundance as an innovative addition to water quality monitoring programs. *Ocean Science*, *15*(5), 1267–1285. https://doi.org/10.5194/os-15-1267-2019

Alou-Font, E., Roy, S., Agusti, S., & Gosselin, M. (2016). Cell viability, pigments and photosynthetic performance of Arctic phytoplankton in contrasting ice-covered and open-water conditions during the spring-summer transition. *Marine Ecology Progress Series*, *543*, 89–106. https://doi.org/10.3354/meps11562

Arrigo, K. R. (2005). Marine microorganisms and global nutrient cycles. *Nature*, *437*(7057), 349–355. https://doi.org/10.1038/nature04159

Arrigo, K. R., van Dijken, G., & Pabi, S. (2008). Impact of a shrinking Arctic ice cover on marine primary production. *Geophysical Research Letters*, *35*, L19603. https://doi.org/10.1029/2008GL035028

Arrigo, K. R., & van Dijken, G. L. (2015). Continued increases in Arctic Ocean primary production. *Progress in Oceanography*, *136*, 60–70. https://doi.org/10.1016/j.pocean.2015.05.002

Behrenfeld, M. J., & Kolber, Z. S. (1999). Widespread iron limitation of phytoplankton in the south pacific ocean. *Science*, *283*(5403), 840–843. https://doi.org/10.1126/science.283.5403.840

Behrenfeld, M. J., Prasil, O., Kolber, Z. S., Babin, M., & Falkowski, P. G. (1998). Compensatory changes in photosystem II electron turnover rates protect photosynthesis from photoinhibition. *Photosynthesis Research*, *58*(3), 259–268. https://doi.org/10.1023/A:1006138630573

Bibby, T. S., Gorbunov, M. Y., Wyman, K. W., & Falkowski, P. G. (2008). Photosynthetic community responses to upwelling in mesoscale eddies in the subtropical North Atlantic and Pacific Oceans. *Deep-Sea Research Part Ii-Topical Studies in Oceanography*, *55*(10–13), 1310–1320. https://doi.org/10.1016/j.dsr2.2008.01.014

Boyd, P. W. (2019). Physiology and iron modulate diverse responses of diatoms to a warming Southern Ocean. *Nature Climate Change*, *9*(2), 148. https://doi.org/10.1038/s41558-018-0389-1

Carmack, E. C., Yamamoto-Kawai, M., Haine, T. W. N., Bacon, S., Bluhm, B. A., Lique, C., et al. (2016). Freshwater and its role in the Arctic marine system: Sources, disposition, storage, export, and physical and biogeochemical consequences in the Arctic and global oceans. *Journal of Geophysical Research: Biogeosciences*, *121*, 675–717. https://doi.org/10.1002/2015JG003140

Cermeño, P., Estévez-Blanco, P., Marañón, E., & Fernóndez, E. (2005). Maximum photosynthetic efficiency of size-fractionated phytoplankton assessed by14C uptake and fast repetition rate fluorometry. *Limnology and Oceanography*, *50*(5), 1438–1446. https://doi.org/10.4319/lo.2005.50.5.1438

Cloern, J. E., Grenz, C., & VidergarLucas, L. (1995). An empirical model of the phytoplankton chlorophyll:carbon ratio—The conversion factor between productivity and growth rate. *Limnology and Oceanography*, *40*(7), 1313–1321. https://doi.org/10.4319/lo.1995.40.7.1313

Codispoti, L. A., Flagg, C., Kelly, V., & Swift, J. H. (2005). Hydrographic conditions during the 2002 SBI process experiments. *Deep-Sea Research Part Ii-Topical Studies in Oceanography*, *52*(24–26), 3199–3226. https://doi.org/10.1016/j.dsr2.2005.10.007

Coello-Camba, A., & Agustí, S. (2017). Thermal thresholds of phytoplankton growth in polar waters and their consequences for a warming Polar Ocean. *Frontiers in Marine Science*, *4*(168). https://doi.org/10.3389/fmars.2017.00168

Coupel, P., Jin, H. Y., Joo, M., Horner, R., Bouvet, H. A., Sicre, M. A., et al. (2012). Phytoplankton distribution in unusually low sea ice cover over the Pacific Arctic. *Biogeosciences*, *9*(11), 4835–4850. https://doi.org/10.5194/bg-9-4835-2012

Coupel, P., Ruiz-Pino, D., Sicre, M. A., Chen, J. F., Lee, S. H., Schiffrine, N., et al. (2015). The impact of freshening on phytoplankton production in the Pacific Arctic Ocean. *Progress in Oceanography*, *131*, 113–125. https://doi.org/10.1016/j.pocean.2014.12.003

Cullen, J. J. (1982). The deep chlorophyll maximum: Comparing vertical profiles of chlorophyll a. *Canadian Journal of Fisheries and Aquatic Sciences*, *39*(5), 791–803. https://doi.org/10.1139/f82-108

Danielson, S. L., Eisner, L., Ladd, C., Mordy, C., Sousa, L., & Weingartner, T. J. (2017). A comparison between late summer 2012 and 2013 water masses, macronutrients, and phytoplankton standing crops in the northern Bering and Chukchi seas. *Deep-Sea Research Part Ii-Topical Studies in Oceanography*, *135*, 7–26. https://doi.org/10.1016/j.dsr2.2016.05.024

Falkowski, P. G., Greene, R. M., & Geider, R. J. (1992). Physiological limitations on phytoplankton productivity in the ocean. *Oceanography*, *5*(2), 84–91.

Falkowski, P. G., & Kolber, Z. (1995). Variations in chlorophyll fluorescence yields in phytoplankton in the world oceans. *Australian Journal of Plant Physiology*, *22*(2), 341–355. https://doi.org/10.1071/Pp9950341

Falkowski, P. G., & Raven, J. A. (2007). *Aquatic photosynthesis*, Princeton, NJ: Princeton University Press.

Frey, K. E., Maslanik, J. A., Kinney, J. C., & Maslowski, W. (2014). Recent variability in sea ice cover, age, and thickness in the Pacific Arctic region. In J. Grebmeier & W. Maslowski (Eds.), *The Pacific Arctic region*(31–63). Dordrecht: Springer.

Fujiwara, A., Hirawake, T., Suzuki, K., Eisner, L., Imai, I., Nishino, S., et al. (2016). Influence of timing of sea ice retreat on phytoplankton size during marginal ice zone bloom period on the Chukchi and Bering shelves. *Biogeosciences*, *13*(1), 115–131. https://doi.org/10.5194/bg-13-115-2016

Furuya, K., Hasegawa, O., Yoshikawa, T., & Taguchi, S. (1998). Photosynthesis-irradiance relationship of phytoplankton and primary production in the vicinity of Kuroshio warm core ring in spring. *Journal of Oceanography*, *54*(5), 545–552. https://doi.org/10.1007/bf02742456

Geider, R. J. (1987). Light and temperature-dependence of the carbon to chlorophyll-a ratio in microalgae and cyanobacteria—Implications for physiology and growth of phytoplankton. *New Phytologist*, *106*(1), 1–34. https://doi.org/10.1111/j.1469-8137.1987.tb04788.x

Geider, R. J., Laroche, J., Greene, R. M., & Olaizola, M. (1993). Response of the photosynthetic apparatus of phaeodactylum-tricornutum (Bacillariophyceae) to nitrate, phosphate, or iron starvation. *Journal of Phycology*, *29*(6), 755–766. https://doi.org/10.1111/j.0022-3646.1993.00755.x

Geider, R. J., Platt, T., & Raven, J. A. (1986). Size dependence of growth and photosynthesis in diatoms—A synthesis. *Marine Ecology Progress Series*, *30*(1), 93–104. https://doi.org/10.3354/meps030093

Gorbunov, M. Y., & Falkowski, P. G. (2004). Flourescnece induction and relaxation (FIRE) technique and instrumentation for monitoring photosynthetic processes and primary production in aquatic ecosystems. In *Photosynthesis: Fundamental aspects to global perspectives—Proceedings of the 13th International Congress of Photosynthesis* (pp. 1029–1031). Montreal: Allen Press.

Gorbunov, M. Y., & Falkowski, P. G. (2020). Using chlorophyll fluorescence kinetics to determine photosynthesis in aquatic ecosystem. *Limnology and Oceanography*. https://doi.org/10.1002/lno.11581

Gorbunov, M. Y., Falkowski, P. G., & Kolber, Z. S. (2000). Measurement of photosynthetic parameters in benthic organisms in situ using a SCUBA-based fast repetition rate fluorometer. *Limnology and Oceanography*, *45*(1), 242–245. https://doi.org/10.4319/lo.2000.45.1.0242

Gorbunov, M. Y., Kolber, Z. S., & Falkowski, P. G. (1999). Measuring photosynthetic parameters in individual algal cells by fast repetition rate fluorometry. *Photosynthesis Research*, *62*(2–3), 141–153. https://doi.org/10.1023/A:1006360005033

Gorbunov, M. Y., Kolber, Z. S., Lesser, M. P., & Falkowski, P. G. (2001). Photosynthesis and photoprotection in symbiotic corals. *Limnology and Oceanography*, *46*(1), 75–85. https://doi.org/10.4319/lo.2001.46.1.0075

Gorbunov, M. Y., Shirsin, E., Nikonova, E., Fadeev, V. V., & Falkowski, P. G. (2020). The use of multi-spectral fluorescence induction and relaxation technique for physiological and taxonomic analysis of phytoplankton communities. *Marine Ecology Progress Series*. https://doi.org/10.3354/meps13358

Graversen, R. G., Mauritsen, T., Tjernstrom, M., Kallen, E., & Svensson, G. (2008). Vertical structure of recent Arctic warming. *Nature*, *451*(7174), 53–56. https://doi.org/10.1038/nature06502

Graziano, L. M., Geider, R. J., Li, W. K. W., & Olaizola, M. (1996). Nitrogen limitation of North Atlantic phytoplankton: Analysis of physiological condition in nutrient enrichment experiments. *Aquatic Microbial Ecology*, *11*(1), 53–64. https://doi.org/10.3354/ame011053

Hein, M., Pedersen, M. F., & Sandjensen, K. (1995). Size-dependent nitrogen uptake in micro- and macroalgae. *Marine Ecology Progress Series*, *118*(1–3), 247–253. https://doi.org/10.3354/meps118247

Jassby, A. D., & Platt, T. (1976). Mathematical formulation of the relationship between photosynthesis and light for phytoplankton. *Limnology and Oceanography*, *21*(4), 540–547. https://doi.org/10.4319/lo.1976.21.4.0540

Kipp, L. E., Charette, M. A., Moore, W. S., Henderson, P. B., & Rigor, I. G. (2018). Increased fluxes of shelf-derived materials to the central Arctic Ocean. *Science Advances*, *4*(1), eaao1302. https://doi.org/10.1126/sciadv.aao1302

Kirk, J. T. O. (1994). *Light and photosynthesis in aquatic ecosystems*. Cambridge: Cambridge University Press.

Kolber, Z., Zehr, J., & Falkowski, P. (1988). Effects of growth irradiance and nitrogen limitation on photosynthetic energy conversion in photosystem II. *Plant Physiology*, *88*(3), 923–929. https://doi.org/10.1104/pp.88.3.923

Kolber, Z. S., Barber, R. T., Coale, K. H., Fitzwater, S. E., Greene, R. M., Johnson, K. S., et al. (1994). Iron limitation of phytoplankton photosynthesis in the equatorial Pacific-Ocean. *Nature*, *371*(6493), 145–149. https://doi.org/10.1038/371145a0

Kolber, Z. S., & Falkowski, P. G. (1993). Use of active fluorescence to estimate phytoplankton photosynthesis in-situ. *Limnology and Oceanography*, *38*(8), 1646–1665. https://doi.org/10.4319/lo.1993.38.8.1646

Kolber, Z. S., Prasil, O., & Falkowski, P. G. (1998). Measurements of variable chlorophyll fluorescence using fast repetition rate techniques: Defining methodology and experimental protocols. *Biochimica et Biophysica Acta-Bioenergetics*, *1367*(1–3), 88–106. https://doi.org/10.1016/S0005-2728(98)00135-2

Kulk, G., van de Poll, W. H., & Buma, A. G. J. (2018). Photophysiology of nitrate limited phytoplankton communities in Kongsfjorden, Spitsbergen. *Limnology and Oceanography*, *63*(6), 2606–2617. https://doi.org/10.1002/lno.10963

Lee, Y., Min, J. O., Yang, E. J., Cho, K. H., Jung, J., Park, J., et al. (2019). Influence of sea ice concentration on phytoplankton community structure in the Chukchi and East Siberian Seas, Pacific Arctic Ocean. *Deep-Sea Research Part I-Oceanographic Research Papers*, *147*, 54–64. https://doi.org/10.1016/j.dsr.2019.04.001

Lewis, K. M., Arntsen, A. E., Coupel, P., Joy-Warren, H., Lowry, K. E., Matsuoka, A., et al. (2019). Photoacclimation of Arctic Ocean phytoplankton to shifting light and nutrient limitation. *Limnology and Oceanography*, *64*(1), 284–301. https://doi.org/10.1002/lno.11039

Lewis, K. M., van Dijken, G. L., & Arrigo, K. R. (2020). Changes in phytoplankton concentration now drive increased Arctic Ocean primary production. *Science*, *369*(6500), 198–202. https://doi.org/10.1126/science.aay8380

Lin, H., Kuzminov, F. I., Park, J., Lee, S., Falkowski, P. G., & Gorbunov, M. Y. (2016). Phytoplankton. The fate of photons absorbed by phytoplankton in the global ocean. *Science*, *351*(6270), 264–267. https://doi.org/10.1126/science.aab2213

Lindemann, C., Fiksen, O., Andersen, K. H., & Aksnes, D. L. (2016). Scaling Laws in phytoplankton nutrient uptake affinity. *Frontiers in Marine Science*, *3*(26) UNSP 26. https://doi.org/10.3389/fmars.2016.00026

Lowry, K. E., Pickart, R. S., Mills, M. M., Brown, Z. W., van Dijken, G. L., Bates, N. R., & Arrigo, K. R. (2015). The influence of winter water on phytoplankton blooms in the Chukchi Sea. *Deep-Sea Research Part Ii-Topical Studies in Oceanography*, *118*, 53–72. https://doi.org/10.1016/j.dsr2.2015.06.006

Martin, J. H., Coale, K. H., Johnson, K. S., Fitzwater, S. E., Gordon, R. M., Tanner, S. J., et al. (1994). Testing the iron hypothesis in ecosystems of the equatorial Pacific-Ocean. *Nature*, *371*(6493), 123–129. https://doi.org/10.1038/371123a0

McMinn, A., & Hegseth, E. N. (2004). Quantum yield and photosynthetic parameters of marine microalgae from the southern Arctic Ocean, Svalbard. *Journal of the Marine Biological Association of the United Kingdom*, *84*(5), 865–871. https://doi.org/10.1017/S0025315404010112h

McPhee, M. G., Proshutinsky, A., Morison, J. H., Steele, M., & Alkire, M. B. (2009). Rapid change in freshwater content of the Arctic Ocean. *Geophysical Research Letters*, *36*, L10602. https://doi.org/10.1029/2009GL037525

Mills, M. M., Brown, Z. W., Laney, S. R., Ortega-Retuerta, E., Lowry, K. E., van Dijken, G. L., & Arrigo, K. R. (2018). Nitrogen limitation of the summer phytoplankton and heterotrophic prokaryote communities in the Chukchi Sea. *Frontiers in Marine Science*, *5*(362) UNSP 362. https://doi.org/10.3389/fmars.2018.00362

Moore, C. M., Lucas, M. I., Sanders, R., & Davidson, R. (2005). Basin-scale variability of phytoplankton bio-optical characteristics in relation to bloom state and community structure in the Northeast Atlantic. *Deep-Sea Research Part I-Oceanographic Research Papers*, *52*(3), 401–419. https://doi.org/10.1016/j.dsr.2004.09.003

Moore, C. M., Mills, M. M., Arrigo, K. R., Berman-Frank, I., Bopp, L., Boyd, P. W., et al. (2013). Processes and patterns of oceanic nutrient limitation. *Nature Geoscience*, *6*(9), 701–710. https://doi.org/10.1038/Ngeo1765

Moore, C. M., Mills, M. M., Langlois, R., Milne, A., Achterberg, E. P., La Roche, J., & Geider, R. J. (2008). Relative influence of nitrogen and phosphorous availability on phytoplankton physiology and productivity in the oligotrophic sub-tropical North Atlantic Ocean. *Limnology and Oceanography*, *53*(1), 291–305. https://doi.org/10.4319/lo.2008.53.1.0291

Mosharov, S. A., Sergeeva, V. M., Kremenetskiy, V. V., Sazhin, A. F., & Stepanova, S. V. (2019). Assessment of phytoplankton photosynthetic efficiency based on measurement of fluorescence parameters and radiocarbon uptake in the Kara Sea. *Estuarine, Coastal and Shelf Science*, *218*, 59–69. https://doi.org/10.1016/j.ecss.2018.12.004

Park, J., Kuzminov, F. I., Bailleul, B., Yang, E. J., Lee, S., Falkowski, P. G., & Gorbunov, M. Y. (2017). Light availability rather than Fe controls the magnitude of massive phytoplankton bloom in the Amundsen Sea polynyas, Antarctica. *Limnology and Oceanography*, *62*(5), 2260–2276. https://doi.org/10.1002/lno.10565

Parkhill, J. P., Maillet, G., & Cullen, J. J. (2001). Fluorescence-based maximal quantum yield for PSII as a diagnostic of nutrient stress. *Journal of Phycology*, *37*(4), 517–529. https://doi.org/10.1046/j.1529-8817.2001.037004517

Parsons, T. R., Maita, Y., & Lalli, C. M. (1984). *A manual of chemical and biological methods for seawater analysis*, Amsterdam: Pergamon Press.

Pickart, R. S., Pratt, L. J., Torres, D. J., Whitledge, T. E., Proshutinsky, A. Y., Aagaard, K., et al. (2010). Evolution and dynamics of the flow through herald canyon in the western Chukchi Sea. *Deep-Sea Research Part Ii-Topical Studies in Oceanography*, *57*(1–2), 5–26. https://doi.org/10.1016/j.dsr2.2009.08.002

Pisareva, M. N., Pickart, R. S., Lin, P. G., Fratantoni, P. S., & Weingartner, T. J. (2019). On the nature of wind-forced upwelling in Barrow canyon. *Deep-Sea Research Part Ii-Topical Studies in Oceanography*, *162*, 63–78. https://doi.org/10.1016/j.dsr2.2019.02.002

Raven, J. A. (1998). The twelfth Tansley lecture. Small is beautiful: The picophytoplankton. *Functional Ecology*, *12*(4), 503–513. https://doi.org/10.1046/j.1365-2435.1998.00233.x

Rhee, G. u., & Gotham, I. J. (1981). The effect of environmental factors on phytoplankton growth: Light and the interactions of light with nitrate limitation1. *Limnology and Oceanography*, *26*(4), 649–659. https://doi.org/10.4319/lo.1981.26.4.0649

Rijkenberg, M. J. A., Slagter, H. A., van der Loeff, M. R., van Ootien, J., & Gerringa, L. J. A. (2018). Dissolved Fe in the deep and upper Arctic Ocean with a focus on Fe limitation in the Nansen Basin. *Frontiers in Marine Science*, *5*(88), 88UNSP. https://doi.org/10.3389/fmars.2018.00088

Screen, J. A., & Simmonds, I. (2010). The central role of diminishing sea ice in recent Arctic temperature amplification. *Nature*, *464*(7293), 1334–1337. https://doi.org/10.1038/nature09051

Serreze, M. C., & Stroeve, J. (2015). Arctic Sea ice trends, variability and implications for seasonal ice forecasting. *Philosophical Transactions. Series A, Mathematical, Physical, and Engineering Sciences*, *373*(2045), 20140159. https://doi.org/10.1098/rsta.2014.0159

Sieburth, J. M., Smetacek, V., & Lenz, J. (1978). Pelagic ecosystem structure: Heterotrophic compartments of the plankton and their relationship to plankton size fractions 1. *Limnology and Oceanography*, *23*(6), 1256–1263. https://doi.org/10.4319/lo.1978.23.6.1256

Smith, V. H. (1982). The nitrogen and phosphorus dependence of algal biomass in lakes: An empirical and theoretical analysis1. *Limnology and Oceanography*, *27*(6), 1101–1111. https://doi.org/10.4319/lo.1982.27.6.1101

Suggett, D. J., Borowitzka, M. A., & Prášil, O. (2010). *Chlorophyll a fluorescence in aquatic sciences: Methods and applications*. The Netherlands: Springer.

Suggett, D. J., MacIntyre, H. L., & Geider, R. J. (2004). Evaluation of biophysical and optical determinations of light absorption by photosystem II in phytoplankton. *Limnology and Oceanography: Methods*, *2*(10), 316–332. https://doi.org/10.4319/lom.2004.2.316

Suggett, D. J., Moore, C. M., Hickman, A. E., & Geider, R. J. (2009). Interpretation of fast repetition rate (FRR) fluorescence: Signatures of phytoplankton community structure versus physiological state. *Marine Ecology Progress Series*, *376*, 1–19. https://doi.org/10.3354/meps07830

Sugie, K., Fujiwara, A., Nishino, S., Kameyama, S., & Harada, N. (2020). Impacts of temperature, CO2, and salinity on phytoplankton community composition in the Western Arctic Ocean. *Frontiers in Marine Science*, *6*(821), 821. https://doi.org/10.3389/fmars.2019.00821

Timmermans, M. L., Proshutinsky, A., Krishfield, R. A., Perovich, D. K., Richter-Menge, J. A., Stanton, T. P., & Toole, J. M. (2011). Surface freshening in the Arctic Ocean's Eurasian Basin: An apparent consequence of recent change in the wind-driven circulation. *Journal of Geophysical Research*, *116*, C00D03. https://doi.org/10.1029/2011JC006975

Tremblay, J. E., Michel, C., Hobson, K. A., Gosselin, M., & Price, N. M. (2006). Bloom dynamics in early opening waters of the Arctic Ocean. *Limnology and Oceanography*, *51*(2), 900–912. https://doi.org/10.4319/lo.2006.51.2.0900

Uitz, J. U., Huot, Y., Bruyant, F., Babin, M., & Claustre, H. (2008). Relating phytoplankton photophysiological properties to community structure on large scales. *Limnology and Oceanography*, *53*(2), 614–630. https://doi.org/10.4319/lo.2008.53.2.0614

Wang, J., Liu, Q. Z., Jin, M. B., Ikeda, M., & Saucier, F. J. (2005). A coupled ice-ocean model in the pan-Arctic and North Atlantic Ocean: Simulation of seasonal cycles. *Journal of Oceanography*, *61*(2), 213–233. https://doi.org/10.1007/s10872-005-0033-3

Wassmann, P., Duarte, C. M., Agusti, S., & Sejr, M. K. (2011). Footprints of climate change in the Arctic marine ecosystem. *Global Change Biology*, *17*(2), 1235–1249. https://doi.org/10.1111/j.1365-2486.2010.02311.x

Woodgate, R. A., & Aagaard, K. (2005). Revising the Bering Strait freshwater flux into the Arctic Ocean. *Geophysical Research Letters*, *32*, L02602. https://doi.org/10.1029/2004GL021747

Xu, K., Fu, F. X., & Hutchins, D. A. (2014). Comparative responses of two dominant Antarctic phytoplankton taxa to interactions between ocean acidification, warming, irradiance, and iron availability. *Limnology and Oceanography*, *59*(6), 1919–1931. https://doi.org/10.4319/lo.2014.59.6.1919

Yun, M. S., Whitledge, T. E., Stockwell, D., Son, S. H., Lee, J. H., Park, J. W., et al. (2016). Primary production in the Chukchi Sea with potential effects of freshwater content. *Biogeosciences*, *13*(3), 737–749. https://doi.org/10.5194/bg-13-737-2016

Zhu, Y. L., Suggett, D. J., Liu, C. G., He, J. F., Lin, L. S., Le, F. F., et al. (2019). Primary productivity dynamics in the summer Arctic Ocean confirms broad regulation of the Electron requirement for carbon fixation by light-phytoplankton community interaction. *Frontiers in Marine Science*, *6*(275), UNSP 275. https://doi.org/10.3389/fmars.2019.00275